



Originally published as:

Trumbull, R. B., Krienitz, M.-S., Grundmann, G., Wiedenbeck, M. (2009): Tourmaline geochemistry and  $\delta^{11}\text{B}$  variations as a guide to fluid-rock interaction in the Habachtal emerald deposit, Tauern Window, Austria. - *Contributions to Mineralogy and Petrology*, 157, 3, 411-427

DOI: [10.1007/s00410-008-0342-9](https://doi.org/10.1007/s00410-008-0342-9)

1 **Tourmaline geochemistry and  $\delta^{11}\text{B}$  variations as a guide to fluid-rock interaction in the**  
2 **Habachtal emerald deposit, Tauern Window, Austria**

3  
4  
5  
6 **R.B. Trumbull<sup>1</sup>, M.-S. Krienitz<sup>1</sup>, G. Grundmann<sup>2</sup>, M. Wiedenbeck<sup>1</sup>**

7 1 GFZ German Research Centre for Geosciences, Telegrafenberg, 14473 Potsdam, Germany

8 2 Technical University of Munich, Arcistrasse 21, 80333 Munich, Germany

9  
10 **Abstract**

11 Tourmalines from the Habachtal emerald deposit in the Eastern Alps formed together with  
12 emerald in a ductile shear zone during blackwall metasomatism between pelitic country rocks  
13 and a serpentinite body. Electron microprobe and secondary ion mass spectrometric (SIMS)  
14 analyses provide a record of chemical and B-isotope variations in tourmalines representing an  
15 idealized profile from metapelites into the blackwall sequence of biotite and chlorite schists.  
16 Tourmaline is intermediate schorl-dravite in the country rock and become increasingly  
17 dravitic in the blackwall zones, while F and Cr contents increase and Al drops. Metasomatic  
18 tourmaline from blackwall zones is typically zoned optically and chemically, with rim  
19 compositions rich in Mg, Ti, Ca and F compared with the cores. The total range in  $\delta^{11}\text{B}$   
20 values is -13.8 to -5.1‰ and the within-sample variations are typically 3 to 5‰. Both of these  
21 ranges are beyond the reach of closed-system fractionation at the estimated 500-550°C  
22 conditions of formation, and at least two boron components with contrasting isotopic  
23 composition are indicated. A key observation from tourmaline core analyses is a systematic  
24 shift in  $\delta^{11}\text{B}$  from the country rock (-14 to -10‰) to the inner blackwall zones (-9 to -5‰).  
25 We suggest that two separate fluids were channeled and partially mixed in the Habachtal  
26 shear zone during blackwall alteration and tourmaline-emerald mineralization. A regional  
27 metamorphic fluid carried isotopically light boron as observed in the metapelite country  
28 rocks. The other fluid is derived from the serpentinite association and has isotopically heavier  
29 boron typical for MORB or altered oceanic crust.

30  
31 **Keywords:**

32 SIMS, B-isotopes, tourmaline, sector zoning, blackwall alteration, Eastern Alps

## 1 **1. Introduction**

2 Ultramafic rocks caught up in collisional orogens like the Himalayan-Alpine chain commonly  
3 end up as dismembered bodies of serpentinite strung out along regional shear zones. The  
4 combination of intense deformation and fluid channelling in these zones, along with the  
5 strong geochemical contrast between serpentinite and crustal wallrocks can produce a  
6 particularly vivid form of fluid-rock interaction known as blackwall zoning (Philips and Hess,  
7 1936; Curtis and Brown, 1969; Bucher et al., 2005). Excellent examples of this are exposed in  
8 the Tauern Window of the Eastern Alps, where the additional factors of regional  
9 metamorphism and ductile deformation led to development of spectacular metasomatic rock  
10 assemblages in which the processes of mid-crustal shearing and fluid-rock interaction are well  
11 preserved (Morteani, 1974; Okrusch et al, 1981; Grundmann and Morteani, 1982; Barnes et  
12 al., 2004). Blackwall zoning has also been described in subduction zone melange associations  
13 (e.g., Bebout and Barton, 2002; King et al., 2003; Altherr et al., 2004; Marschall et al., 2006).  
14 The latter two examples are of particular relevance to the present study because tourmaline  
15 formed in the blackwall zones and its chemical and B-isotopic compositions were used to  
16 shed light on the nature of subduction zone fluids.

17 The subject of this paper is a well-studied example of blackwall zoning in the Habachtal  
18 locality in the eastern Tauern Window, which has the distinction of hosting one of Europe's  
19 few important emerald deposits. Habachtal emeralds were systematically mined from  
20 underground workings from the early 1860s until 1939, with a peak production of 68,000  
21 carats in 1903 (Grundmann, 1991). Detailed microtextural and geochemical studies of the  
22 emeralds and their host rocks (Grundmann and Morteani, 1982; 1989) established that  
23 emerald formation was related to blackwall metasomatism in a regional shear zone that  
24 juxtaposed serpentinite and aluminous country rocks. Tourmaline is part of the same mineral  
25 paragenesis as emerald in the blackwall zones and it also occurs in the garnet-mica schists  
26 from outside the shear zone. The blackwall tourmalines are optically zoned and show  
27 distinctive changes in the abundance and internal fabric of mineral inclusions from core to rim  
28 that are also found in emerald porphyroblasts in the same rocks. Tourmaline is more  
29 widespread than emerald in these rocks and its large chemical variability makes it a  
30 potentially valuable monitor of fluid-rock interaction in the blackwall zones. The present  
31 study sets out to document the chemical and B-isotopic variations of tourmalines from an  
32 idealized profile from the country rocks into the blackwall zones. Although the Habachtal  
33 metasomatic rocks and similar units from the Tauern Window have been the subject of many

1 geochemical and petrologic studies in the past, this is the first investigation of tourmaline  
2 compositions.

3

## 4 **2. Geological setting**

5 The Habachtal emerald deposit is situated in the Tauern Window of the Eastern Alps, where  
6 late Paleozoic (Variscan) Penninic units from beneath the Austroalpine nappes are exposed  
7 (Fig. 1a). The deposit is hosted in a regional shear zone that developed along the contact  
8 between granodiorite orthogneisses of the the “Zentralgneis” massif (with U-Pb zircon age of  
9  $314 \pm 7$  Ma, Cliff, 1981) and a variegated metamorphic sequence called the Habach Group  
10 (metapelites and metavolcanics, with local serpentinite bodies). Structurally, the Habach  
11 Group is part of the lower schist cover, which is interpreted as a nappe emplaced above the  
12 Zentralgneis during the Alpine orogeny (Sm-Nd garnet ages of  $30 \pm 1$  Ma, Christensen et al.,  
13 1994). Cutting across the Zentralgneis massif in the Tauern Window is the Greiner zone (Fig.  
14 1a), a ductile shear zone along which the orthogneiss country rocks are locally transformed to  
15 biotite and chlorite schists. Several small bodies of serpentinite also occur along the Greiner  
16 zone (Melcher et al., 2002) and these display the same phenomena of blackwall contact  
17 metasomatism against the felsic country rocks as at Habachtal, but without emerald  
18 mineralization. The deformation and metasomatism along the Greiner zone were studied in  
19 detail by Barnes et al. (2004). They concluded from chemical, stable isotope (O, H) and  
20 mineralogic data that the metasomatizing fluids in the Greiner zone were derived from  
21 serpentinite dehydration. The serpentinites are part of the Penninic units and predate Alpine  
22 metamorphism, whereas the dehydration event and shear deformation are related to the Alpine  
23 event (Barnes et al., 2004). Many of the features described by Barnes et al. (2004) from the  
24 western Tauern Window are also found in the Habachtal locality, which lies along strike of  
25 the Greiner shear zone to the east (Fig. 1a). Textural and petrographic evidence combined  
26 with mineral thermobarometry, O-isotope thermometry and fluid inclusion analysis from  
27 rocks of the Habach Group by Hoernes and Friedrichsen (1974), Grundmann (1989) and Nwe  
28 and Grundmann (1990) documented both a pre-Alpine and an Alpine tectono-metamorphic  
29 event. According to these studies, the peak P-T conditions of the pre-Alpine event were about  
30 300 MPa and 450°C, whereas the Alpine event reached higher grade (450-600 MPa and 500°-  
31 550°C) and partially overprinted the earlier assemblages.

32 The lithologic sequence of blackwall alteration zones at Habachtal comprises the  
33 following rock types, progressing from the serpentinite body to the pelitic schists of the  
34 Habach Group to the SE (Fig. 1b): antigorite-serpentinite, talc schist, talc-actinolite schist,

1 chlorite schist, biotite schist, biotite-albite schist, and garnet-mica schist. Note that this  
2 sequence is idealized from several profiles across the deposit, and in reality the intense shear  
3 deformation has produced a tectonic *mélange* with extreme local variations in thickness of the  
4 zones and intensity of metasomatism. Based on whole-rock geochemical profiles across the  
5 blackwall zones, Grundmann (1983) and Grundmann and Morteani (1989) placed the original  
6 contact of the serpentinite and wallrocks at the present boundary between the chlorite zone  
7 and the talc-actinolite zone. Blackwall alteration is developed on both sides of the serpentinite  
8 body, (Fig. 1b), but beryl and tourmaline occur only on the SE side of the profile, where the  
9 country rocks are pelitic schists of the Habach Group.

10 Detailed microtextural studies of tourmaline, emerald and plagioclase porphyroblasts by  
11 Morteani and Grundmann (1977), Grundmann (1983; 1989), Grundmann and Morteani (1982;  
12 1989) have established a deformation-crystallization history for the Habachtal rocks,  
13 summarized in Figure 3, all of which is related to the Alpine event. An early, syn-  
14 deformational prograde phase is recorded by inclusion-rich and locally rotated crystal cores.  
15 This was followed by at least one higher-temperature and largely post-deformational phase  
16 which is marked in the crystals by inclusion-free rims. Barnes et al. (2004), in their study of  
17 metasomatic rocks from the Greiner zone west of Habachtal, also concluded that the peak  
18 metamorphic conditions followed the main deformation event. Also associated with the  
19 prograde, post-deformational phase at Habachtal was the formation of massive quartz veins  
20 up to 2 meters thick and 200 meters in outcrop extent in the talc schist on the NW side of the  
21 profile (Fig. 1b). Finally, a retrograde metamorphic phase in these rocks involved brittle  
22 deformation with formation of albite, chlorite and biotite.

23 Information about the fluid composition and conditions of emerald formation comes  
24 from a detailed fluid inclusion study by Nwe and Grundmann (1990), who distinguished an  
25 early and late generation of primary inclusions based on their position in zoned emerald  
26 porphyroblasts. These two fluid generations differ significantly in terms of bulk density and  
27 the proportion of CO<sub>2</sub> ( $X_{\text{CO}_2} < 4$  vol.% in the early generation and up to 11 vol.% in later  
28 fluids). The relative increase in CO<sub>2</sub> in later fluids was attributed to consumption of H<sub>2</sub>O by  
29 prograde hydration reactions in the blackwall alteration process (see discussion below).  
30 Microthermometry data allowed construction of a temperature-pressure-time path which  
31 demonstrated that mineral growth was prograde, with formation of the crystal rims at  
32 temperatures corresponding to the peak Alpine metamorphism (500-550°C).

33  
34

### 1 **3. Petrography of the tourmaline samples**

2 The distribution of samples selected for this study is shown on an idealized sketch of the  
3 blackwall sequence in Figure 2. We distinguish three groups of samples, representing the  
4 main host lithologies from unaltered country rocks into the emerald-bearing blackwall  
5 alteration zones, as follows:

- 6 1. The country rock unit, of garnet-mica schist with lenses of plagioclase-biotite gneiss,  
7 which forms a layer up to 2 meters thick within the Habach Group. It contains  
8 tourmaline and quartz-rich stringers and lenses up to 3 cm thick which are parallel to  
9 foliation and often finely-folded. The tourmaline in this unit generally forms dark  
10 brown to black isolated grains or fine grained, massive aggregates of up to 2 cm in  
11 size. It is represented in this study by sample 103-b.
- 12 2. A transitional zone between unaltered garnet-mica schist and the blackwall rocks. The  
13 transition zone rocks sampled for this study are white to light gray albite-muscovite  
14 schist (sample M26) and light gray to dark brown biotite-muscovite schist (AST-2),  
15 which form irregular medium to very fine grained layers and boudinaged lenses  
16 between the garnet mica schist and the blackwall zones. The tourmaline in these rocks  
17 typically forms dark brown to black, fine-grained aggregates up to 2 cm in size, which  
18 are parallel to the main foliation. Isolated columnar or acicular crystals also occur and  
19 clumps of these reach up to 4 cm in length.
- 20 3. The blackwall alteration zones, consisting of biotite- and chlorite-schists which form  
21 irregular lenses and layers up to 1 meter in thickness. The tourmaline in these samples  
22 is dark brown to black and generally forms medium to fine grained, isolated, needle-  
23 like crystals and crystal groups of up to 5 cm in length which are homogeneously  
24 distributed without distinct preferred orientation. Our blackwall samples represent  
25 biotite schist (103-c), biotite-chlorite schist (sample 102) and chlorite schist (103-a).  
26 Sample 102 is noteworthy because tourmaline is found as inclusions in emerald  
27 porphyroblasts.

28

29 Establishing the relationship of tourmaline growth to the sequence of deformation,  
30 metamorphism and blackwall alteration is vital for interpreting of the geochemical results so  
31 it is useful to summarize the textural evidence here. As mentioned above, the metamorphic  
32 rocks at Habachtal underwent two main events of regional metamorphism (Variscan and  
33 Alpine). The ductile shearing and metasomatism which produced blackwall alteration and  
34 mineralization was related to the Alpine event.

1           Tourmaline from garnet-mica schist outside the mineralized shear zone typically forms  
2 crystal aggregates of light to dark brown, euhedral to anhedral crystals. Individual grain sizes  
3 range between 0.01 and 1 mm in diameter. Color zoning is weak and there are only few  
4 mineral inclusions. The mineral assemblage with tourmaline includes quartz, biotite,  
5 plagioclase, titanite, garnet, ilmenite, pyrite, pyrrhotite, apatite, zircon and graphite. Locally,  
6 larger tourmaline grains of this type show two phases of growth where the rocks have been  
7 affected by Alpine-age deformation. The clearest examples of this are where large, brown  
8 tourmaline grains are fractured by the Alpine deformation and show overgrowths and crack-  
9 fillings of lighter brown-blue tourmaline (Fig. 4a, b). In other cases, the younger tourmaline is  
10 recognized as fine-grained polygonal aggregates that formed at the expense of older  
11 tourmaline due to strain-induced grain boundary migration and size reduction (Fig. 4c, d).

12           A very different variety of tourmaline is typical for the blackwall alteration zones  
13 (biotite schist, chlorite schist). In these rocks, tourmaline occurs as isolated, non-oriented,  
14 euhedral porphyroblasts, which are commonly strongly zoned optically and contain abundant  
15 mineral inclusions, particularly in the cores. Typical grain size range between 0.1 mm to 1  
16 mm in diameter and 1 to 10 mm in length. This variety occurs alongside variety one in the  
17 transitional sample AST-2 where it is the only one found in M-26 and in the blackwall  
18 samples. The detailed study of microtextures in tourmaline, emerald and plagioclase  
19 porphyroblasts from the Habachtal blackwall rocks by Grundmann (1983) found that all three  
20 phases show the same sequence of crystal growth and internal fabric development which  
21 indicate the main phase of growth (inclusion-rich cores) during the Alpine deformation and a  
22 later, more static growth of crystal rims. A synoptic sketch is shown in Figure 3 and examples  
23 from the samples in this study are shown in Figures 4e and 4f. The color zoning in blackwall  
24 tourmalines is striking and commonly complex, with up to 6 more or less sharply separate  
25 zones distinguished by yellow-green, blue-green, olive-green, light-brown, dark-brown and  
26 light-blue hues. A special feature of tourmalines from the biotite and chlorite schists is the  
27 development of hourglass sector zoning (Fig. 4g, h). Sector zoning in tourmaline has recently  
28 attracted attention (van Hinsberg et al., 2006; van Hinsberg and Marschall, 2007; van  
29 Hinsberg and Schumacher, 2007) and more details of the Habachtal occurrence are given  
30 below.

31

## 32 **4. Analytical Methods**

33

### 34 **4.1 Electron microprobe analysis**

1 Tourmaline compositions were determined on polished and carbon-coated 2.5 cm round thin  
2 sections by wavelength-dispersive electron microprobe analyses at the  
3 GeoForschungsZentrum (GFZ) Potsdam. The CAMECA SX-100 microprobe was operated at  
4 15 kV accelerating voltage and 20nA beam current. Natural oxide and silicate mineral  
5 reference materials were used for calibration and data reduction employed the method of  
6 Pouchou and Pichoir (1984). Our procedure for microprobe analysis was to routinely analyze  
7 two or more points from the core and rim portions of optically zoned grains to check for  
8 chemical variations. Tourmaline structural formulae were calculated assuming stoichiometric  
9 3.0 B per formula unit and by normalizing to 15 cations in the tetrahedral and octahedral sites  
10 (T + Z + Y) according to the suggestion of Henry and Dutrow (1996). The structural formulae  
11 are approximate to the extent that our chemical analyses are not complete; we did not  
12 determine B, H<sub>2</sub>O, ferrous/ferric iron ratio, and minor elements such as Li and Zn, which may  
13 be present at sub-wt.% level. X-ray element maps illustrating the hourglass sector zoning of  
14 tourmaline in sample 103a (see Fig. 4h) were collected with the JEOL Hyperprobe JXA-  
15 8500F electron microprobe at the GFZ Potsdam, whose field-emission electron gun permits  
16 an extremely small beam diameter at the sample surface (ca. 80 nanometers for the 15 kV  
17 accelerating voltage and 50 nA beam current used here).

18

#### 19 **4.2 Boron isotope determination**

20 The boron isotope composition of tourmaline was determined by secondary ion mass  
21 spectrometry (SIMS) with the CAMECA ims6f instrument at the GFZ Potsdam. After  
22 electron microprobe analysis, the samples were re-polished with alumina and distilled water  
23 to remove the carbon coat, then ultrasonically cleaned with high purity ethanol and coated  
24 with a ~35 nm thick high purity gold coat. The use of a liquid nitrogen cold trap provided a  
25 secondary ion source pressure in the lower 10<sup>-10</sup> Torr range. For the boron isotopic analyses  
26 the ims6f was set up in Köhler mode and employed a nominally 12.5 kV <sup>16</sup>O<sup>-</sup> primary beam  
27 which was focused to about 10 μm diameter on the sample surface. Wherever size permitted,  
28 both rim and core compositions of individual grains were measured. In two analytical  
29 sessions, the beam current was set at 8 nA or 4 nA, the lower current being required to  
30 maintain count rates for <sup>11</sup>B below 500 kHz. Prior to each analysis, a 3 minute preburn was  
31 used in order to remove the gold coat and to establish equilibrium sputtering conditions. The  
32 mass spectrometer was operated at mass resolving power M/ΔM ≈ 1400, sufficient to separate  
33 the isobaric interference of <sup>10</sup>B<sup>1</sup>H on the <sup>11</sup>B mass station and the <sup>9</sup>Be<sup>1</sup>H peak on <sup>10</sup>B. A 50  
34 μm diameter contrast aperture, an 1800 μm field aperture (equivalent to a 150 μm field of



1 view) and 50 V energy window were used without voltage offset. Each analysis consisted of  
2 100 scans of the sequence  $^{9.95}\text{B}$  background (0.1 seconds per cycle),  $^{10}\text{B}$  (2 s) and  $^{11}\text{B}$  (1 s)  
3 resulting in a total analysis time of about 10 minutes. Instrumental mass fractionation (IMF)  
4 and analytical quality were assessed by replicate analyses of tourmaline reference materials  
5 dravite (HS #108796), elbaite (HS #98144) and schorl (HS #112566) from the Harvard  
6 Mineralogical Museum (Dyar et al. 2001), and tourmaline B4 from Tonarini et al. (2003).  
7 During the analytical sessions the 1 sd individual uncertainties were typically  $\pm 0.3\%$  (Table 1  
8 ) and the repeatability on reference samples averaged 0.6 ‰ (1 sd). The variation in observed  
9 mass fractionation among the different reference samples was 1.4 ‰ on average (Table 1),  
10 which we believe to be the best estimate for the trueness of the data set. Boron isotope  
11 compositions are reported in  $\delta^{11}\text{B}$  notation ( $\delta^{11}\text{B} = \{^{11}\text{B}/^{10}\text{B}_{\text{sample}}^{\text{corr}} / ^{11}\text{B}/^{10}\text{B}_{\text{RM}} - 1\} \times 1000$ )  
12 relative to NBS SRM 951, whose  $^{11}\text{B}/^{10}\text{B}$  ratio is taken as 4.04362 (Cantanzaro et al., 1970).  
13 The results of the boron isotope and chemical analyses are listed in Table 2 and the full set of  
14 microprobe data is available in the electronic repository.

15

## 16 **5. Chemical composition of tourmaline**

17

18 Given that the Habachtal tourmalines grew in metasomatic zones between serpentinite and  
19 pelitic schists, it makes sense to describe their compositional features in terms of the three  
20 sample groups: country rock (103b), transitional samples (M-26, AST-2) and blackwall zones  
21 (biotite schist 102 and 103c, chlorite schist 103a). All tourmalines classify in the alkali group  
22 of Hawthorne & Henry (1999) based on cation proportions in the X-site (Fig. 5a), and they  
23 plot on the Mg-rich side of the schorl-dravite join on the Al-Mg-Fe diagram of Henry and  
24 Guidotti (1985), within the fields for metapelite-metapsammite rocks (Fig. 5b).

25 There are significant compositional differences in tourmaline from the three groups of  
26 host rocks. The Fe/(Fe+Mg) ratio is among the most distinct of these (Fig. 6a), with values  
27 declining from the country rocks to the blackwall biotite and chlorite schist, in good  
28 agreement with the whole-rock ranges shown on the diagram (data from Grundmann, 1983).  
29 One of the two transitional zone samples (biotite-muscovite schist AST-2) has Fe/(Fe+Mg)  
30 ratios intermediate between those in the country rock and blackwall tourmalines as expected  
31 for its position in the sequence. However, the other one (albite-muscovite schist M-26) has the  
32 lowest ratios of all samples. This is thought to reflect the protolith composition and not the  
33 effect of blackwall alteration since the rock represents a fragment of pre-Alpine whiteschist  
34 (G. Morteani, pers. comm., 2008) which is rich in magnesian phengite. Also distinctive of

1 tourmalines from the blackwall zones are their moderate to high fluorine contents, which  
2 contrast with the low or negligible F in tourmalines from the country rock and transitional  
3 samples (Fig. 6b). Further, the blackwall tourmalines show a wide range of Ca and Ti  
4 concentrations (0.2 to 1.4 wt.% CaO and 0.1 to 0.8 wt.% TiO<sub>2</sub>) with a strong positive  
5 correlation between the two (Fig. 6c). The country rock tourmalines have a greater scatter of  
6 TiO<sub>2</sub> and CaO values (Fig. 6c). Note that the whiteschist tourmalines (M-26) form a separate  
7 cluster at low TiO<sub>2</sub> on this diagram. Finally, Al concentrations are higher in tourmalines from  
8 the metapelite country rock than in the blackwall zones (Fig. 7a), and these Al-rich  
9 tourmalines also have relatively high values for the X-site vacancy, up to 30% (Figs. 5a, 7b).  
10 The good correlations of Fe vs. total Al and Fe vs. X-site vacancy in these tourmalines and  
11 the slope of data trends compared with the exchange vectors shown on Figure 7 illustrate the  
12 importance of the "alkali-deficient" exchange component  $\{(Na,Fe)(\square,Al)\}_{-1}$  for charge-  
13 balancing the excess aluminum.

14 One might expect high Cr contents in tourmalines from emerald-bearing blackwall rocks  
15 compared to those in the country rocks and the average values of both groups of samples bear  
16 this out (0.05 wt.% Cr<sub>2</sub>O<sub>3</sub> for blackwall samples, 0.02 wt.% for garnet-mica schist). However,  
17 the scatter is large in the both groups and the maximum Cr<sub>2</sub>O<sub>3</sub> content of blackwall  
18 tourmalines is only a moderate 0.14 wt.% (Appendix A). These values are similar to those of  
19 blackwall-hosted tourmalines studied by Altherr et al. (2004) and Marschall et al. (2006) but  
20 they are quite low compared with tourmalines from other emerald-bearing rocks in the  
21 literature. Seifert et al. (2004) reported maxima of 1 to 2.7 wt.% Cr<sub>2</sub>O<sub>3</sub> from tourmaline  
22 coexisting with emerald in blackwall metasomatic rocks (phlogopite-talc-actinolite) from  
23 Zambia, and tourmalines from the Tsa da Glisza (Regal Ridge) emerald prospects in Yukon  
24 Territory reach similarly high Cr<sub>2</sub>O<sub>3</sub> concentrations, with a maximum of 3.3 wt.% (Groat et  
25 al., 2002; C.G. Galbraith, pers. communication 2008).

#### 27 Compositional zoning as a monitor of blackwall alteration

28  
29 As described above, the pre-Alpine fine-grained grains and grain aggregates from the country  
30 rocks and transition zone samples have weak and simple optical zoning (Fig. 4d), and  
31 microprobe analyses from this type of tourmaline show little or no consistent variations in  
32 core vs. rim compositions (Table 2, Appendix A). On the other hand, most tourmaline grains  
33 from the blackwall schists display distinct optical zoning (Fig. 4e, f) and have systematic  
34 compositional zoning as well. Typically, the rims of zoned grains are enriched in Mg, Ti, Ca  
35 and F relative to the cores (Fig. 8). Rims may show relative depletion in Na, Fe and Al, but

1 the trends for these elements are less regular. Zoned emeralds in these rocks also display  
2 consistent trends of higher Mg/(Mg+Fe) ratios and lower Al contents from core to rim  
3 (Grundmann, 1983).

4 It is significant that the core-to-rim compositional variations in the blackwall  
5 tourmalines mirror the overall changes in tourmaline composition from the country rocks into  
6 the blackwall alteration zones, implying that the compositional changes in zoned grains  
7 record the changing fluid composition as blackwall alteration progresses. The lithologic and  
8 petrographic characteristics of the blackwall sequence support this interpretation. First,  
9 microtextures and inclusion fabric of emerald and tourmaline porphyroblasts indicate that the  
10 main period of growth for both phases was syn-deformational and followed by static growth  
11 of the relatively narrow rims (Fig. 3). This growth is prograde, as indicated by fluid inclusion  
12 microthermometry from zoned emeralds by Nwe and Grundmann (1990), with peak  
13 metamorphic temperatures of 500-550°C. Second, whole-rock geochemistry (Grundmann and  
14 Morteani 1989) established that the original contact between serpentinite and the country  
15 rocks was at the present boundary between chlorite schist and actinolite-talc schists (Fig. 2).  
16 This means that the chlorite and biotite blackwall schists were once metapelites and that their  
17 core-to-rim chemical zonation is equivalent to a time sequence of advancing metasomatism.

18 A special feature of tourmalines from the chlorite-biotite schist (sample 103a) is  
19 hourglass sector zoning (Fig. 4g,h), which is unusual for tourmaline and was described in  
20 detail by van Hinsberg et al. (2006). Although common in tourmalines from sample 103a,  
21 hourglass zonation is not developed in any of the other samples examined in this study. Why  
22 this is so is not known. The sector zoning in tourmaline is interesting because the mineral's  
23 polar properties cause a compositional and color contrast between the C<sup>-</sup> (analogous) and C<sup>+</sup>  
24 (antilogous) poles (Fig. 4g). The sector-zoned tourmalines from sample 103a show the typical  
25 variations in Ti and Ca on opposite ends of the C-axis, leading to a clear color contrast like  
26 those from other localities described by van Hinsberg et al. (2006). We did not perform  
27 detailed microprobe traverses across these crystals but instead illustrate their compositional  
28 variations with a Ti distribution map from a large and well-developed example in Figure 4h.  
29 Spot analyses on this and other zoned grains in the sample demonstrate a contrast in CaO and  
30 TiO<sub>2</sub> concentrations at the C<sup>+</sup> vs. C<sup>-</sup> sectors of about 0.5 wt.%. Henry and Dutrow (1996)  
31 suggested that the bipolar effect is significant only in tourmalines from low-temperature  
32 conditions but the work of van Hinsberg et al. (2006; 2007) shows that zoning can persist to  
33 the amphibolite grade and this is confirmed by the Habachtal tourmalines, which formed at  
34 temperatures of at least 500°C (Nwe and Grundmann, 1990). Van Hinsberg and Marschall

1 (2007) found that sector-zoned tourmaline crystals can show a slight but significant variation  
2 in B-isotope composition between the C<sup>+</sup> and C<sup>-</sup> sectors. Our SIMS analyses on the sector-  
3 zoned Habachtal crystals confirm a weak isotopic effect as described below.

## 5 **6. Boron isotope results**

6 The total range in boron isotope compositions for tourmalines from the country rock  
7 schist to the metasomatic rocks of the blackwall zones is from -13.8 ‰ to -5.1 ‰ in the  $\delta^{11}\text{B}$   
8 notation (Fig. 9, Table 2). These isotopically light values are well within the range of  
9 tourmalines from metasedimentary rocks reported from other studies (Palmer and Swihart,  
10 1986; Kasemann et al., 2000; Bebout and Nakamura, 2003; Trumbull et al., 2008), and they  
11 contrast with the heavy B-isotope values of tourmaline from eclogite-serpentinite mélange  
12 rocks in Turkey (-2.2 to +1.7‰) reported by Altherr et al. (2004), and in Syros (+18 to +28  
13 ‰) found by Marschall et al. (2006). Both of those studies attributed the isotopically heavy  
14 boron to a fluid source in the subducted oceanic slab, which in the case of Syros was further  
15 modified during fluid migration through and interaction with serpentinites above the slab.

16 The most significant features of the Habachtal isotope data are summarized here and  
17 their possible implications for the fluid source and mineralization process are discussed in the  
18 following section.

- 19 1. There is an overall shift in the B-isotope compositions of tourmaline from more negative  
20  $\delta^{11}\text{B}$  values in the country rock samples to less negative values in the blackwall zones  
21 (Fig. 9). The differences in composition between country rock and blackwall zones are  
22 largest and most consistent with respect to the core compositions.
- 23 2. The variations in  $\delta^{11}\text{B}$  within individual samples is typically 3-5 ‰, which is  
24 considerably greater than the analytical uncertainty and therefore an indication for a  
25 heterogeneous boron source and/or processes of isotopic fraction connected with  
26 tourmaline growth in these rocks.
- 27 3. Isotopic variations from core to rim of zoned tourmaline grains were not found in the  
28 country-rock tourmalines, but there are examples of significant isotopic zoning in some  
29 of the transitional zone and blackwall samples (Table 2). The core-rim isotopic contrast  
30 rarely exceeds 2‰; however, the trends of isotope zoning are mostly the same, with  
31 tourmaline rims being isotopically lighter than the cores (Fig. 9). Tourmaline in sample  
32 103a (chlorite schist), which shows the strongest optical and chemical zonation (Fig. 8),  
33 also has the strongest isotopic zonation of all samples, at 4 ‰.

1 4. Tourmaline grains with well-developed hourglass sector zoning in sample 103a were  
2 checked for B-isotope variations by analysing two points on each of the C<sup>+</sup> and C<sup>-</sup>  
3 sectors in two separate grains (Appendix B). The results showed minor but significant  
4 isotopic differences. Specifically, grain “C-T2” (Fig. 4g, h) yielded two identical values  
5 for the C<sup>+</sup> zone (-10.9 ‰) whereas the C<sup>-</sup> values were -12.0 and -12.5 ‰, giving an  
6 average contrast of 1.3 ‰. For grain “D-T1”, the C<sup>+</sup> sector yielded -8.0 and -8.3 ‰ and  
7 the C<sup>-</sup> values were -9.3 and -10.1 ‰, for an average contrast of 1.5 ‰. These differences  
8 exceed both the SIMS repeatability error of about 0.6‰ (Table 1) and the individual  
9 uncertainties calculated by error propagation [ $\sigma_{a+b} = (\sigma_a^2 + \sigma_b^2)^{1/2}$ ]. Furthermore, the  
10 sense of variation is the same in both grains, with isotopically lighter boron at the C<sup>-</sup>  
11 sector, in agreement with the findings of van Hinsberg and Marschall (2007). The  
12 reason for an isotopic contrast between the two sectors is presently not understood and it  
13 deserves further study. However, the effect is too weak to complicate the overall  
14 interpretation of this study and sector zoning affects only one sample.

## 15 16 **7. Discussion: B-isotope variations and implications for the fluid source**

17 Two features of the tourmaline  $\delta^{11}\text{B}$  results stand out as most significant in their  
18 implications for fluid-rock interaction in the Habachtal deposit. The first is the observed  
19 variation by up to 6 ‰ in the isotope composition within individual samples. In many cases  
20 this internal variation is partly due to isotopic zoning, which is typically on the order of 2 ‰  
21 and involves lower  $\delta^{11}\text{B}$  values in rims relative to cores. The strongest isotopic zoning of  
22 about 4 ‰ was found in tourmalines from the inner blackwall zone (chlorite schist 103a),  
23 which is the sample representing the most advanced metasomatism. The second important  
24 feature is a systematic difference in the B-isotope composition depending on location of the  
25 samples in the shear zone/alteration sequence. Tourmaline from the country rock metapelite  
26 has low  $\delta^{11}\text{B}$  values (-13 to -10 ‰), typical for continental crust whereas the blackwall zone  
27 tourmalines are isotopically heavier, reaching -5 ‰ in  $\delta^{11}\text{B}$  (Fig. 9). Furthermore, these  
28 spatial differences among the samples are best developed in the tourmaline core  
29 compositions, as emphasized by the shaded band on Fig. 9, meaning that they relate to the  
30 fluid-rock system during the main stage of tourmaline growth in the shear zone..

31 In principle, the observed B-isotope variations in Habachtal tourmalines can relate to  
32 one or both of two factors: local conditions that cause isotopic fractionation between fluid and  
33 growing crystals (closed-system, single initial fluid composition); or an open-system behavior  
34 with more than one fluid composition controlling the B-isotopes. Obviously, some open

1 system behavior is expected for a ductile shear zone with strong metasomatic alteration and  
2 meter-thick quartz veins, but we will first consider what range of B-isotopic variations can be  
3 expected from fluid-mineral fractionation processes and temperature gradients acting on an  
4 initially constant fluid composition. For the Habachtal rocks, the important minerals to  
5 consider are not only tourmaline but potentially also biotite and chlorite, since the blackwall  
6 biotite and chlorite schists consist of more than 90 vol. % of these minerals. The condition for  
7 partitioning of B-isotopes between phases is a change in the coordination environment of  
8 boron, with  $^{10}\text{B}$  being enriched in tetrahedral sites and  $^{11}\text{B}$  in trigonal coordination. In  
9 addition, the fractionation effect is inversely dependent on temperature. Boron in  
10 hydrothermal fluids occurs in trigonal  $\text{B}(\text{OH})_3$  complexes at the low pH conditions suitable  
11 for tourmaline stability (Palmer and Swihart, 1996; Schmidt et al., 2005). Boron in tourmaline  
12 forms trigonal  $\text{BO}_3$  groups whereas it replaces Al in tetrahedral sites in the sheet silicates.  
13 Experimental studies are available for B-isotope fractionation between fluid-tourmaline  
14 (Palmer et al., 1992; Meyer et al., 2008), fluid-clay (Williams et al., 2001) and fluid-  
15 muscovite (Wunder et al., 2005).

16 Application of the isotope partitioning studies to the Habachtal tourmalines requires  
17 temperature information. The Variscan regional metamorphism in the Tauern Window  
18 reached peak temperatures estimated at  $450^\circ\text{C}$  (Grundmann, 1989). These conditions are  
19 thought to be relevant for tourmalines in the country rock metapelites, whereas the main stage  
20 of tourmaline and emerald growth, along with blackwall alteration and quartz veining in the  
21 Habachtal deposit, took place during Alpine metamorphism, with peak temperatures of about  
22  $550^\circ\text{C}$  (Grundmann, 1989 and references therein). At a temperature of  $550^\circ\text{C}$ , the B-isotope  
23 fractionation between hydrothermal fluid and tourmaline would be about  $-4\text{‰}$  according to  
24 Palmer et al. (1992) or about  $-2\text{‰}$  using the results of Meyer et al. (2008). For comparison,  
25 the fluid-mica fractionation at the same temperature would be about  $-10\text{‰}$  (Wunder et al.,  
26 2005). If we assume for discussion that the  $100^\circ\text{C}$  difference between the Variscan and  
27 Alpine peak conditions is the maximum temperature range to be expected for tourmaline  
28 growth in Habachtal, the corresponding shift in  $\delta^{11}\text{B}$  would be about  $2\text{‰}$  or  $1\text{‰}$  depending on  
29 which experimental results are used. In any case, the expected temperature effect is less than  
30 the within-sample range of  $3\text{--}6\text{‰}$  and much less than the variation of  $8\text{‰}$  between the country  
31 rock and the inner blackwall zone. Also, temperature variations during tourmaline growth can  
32 be ruled out as the cause of isotopic zoning since crystal growth is prograde so the predicted  
33 temperature effect would cause higher  $\delta^{11}\text{B}$  values from core to rim, which is contrary to

1 observation. We conclude that temperature cannot be a controlling factor in the isotopic  
2 variations observed although it may contribute to the scatter of values within samples.

3 Another commonly-cited mechanism for changing the isotopic composition of  
4 tourmaline is a Rayleigh-type fractionation, whereby mineral growth depletes the fluid  
5 reservoir in boron and preferentially in  $^{10}\text{B}$ , causing progressively heavier B-isotopic  
6 compositions in the remaining fluid and late-stage tourmalines. Rayleigh fractionation was  
7 invoked to explain isotopic zoning in tourmalines by Trumbull et al. (2008) but it is not likely  
8 to be significant for the Habachtal example because of the high fluid/rock ratios evidenced by  
9 monomineralic chlorite and biotite schist zones and meter-wide quartz veins. Moreover, the  
10 observed isotopic variation in zoned tourmalines argues against Rayleigh fractionation  
11 because that process should cause isotopically heavier tourmaline rims, whereas zoned grains  
12 show the opposite trends.

13 We have shown that the observed shifts in B-isotopic composition among the Habachtal  
14 samples and within zoned grains cannot be explained by fractionation processes or  
15 temperature gradients alone and so there must be significant time-space variations in the  
16 fluids of contrasting B-isotope composition. There is independent evidence for changing fluid  
17 compositions at Habachtal from a study of fluid inclusions in zoned emerald crystals by Nwe  
18 and Grundmann (1990). These authors distinguished an early and late generation of primary  
19 inclusions which differ primarily in terms of fluid density and the proportion of  $\text{CO}_2$  ( $X_{\text{CO}_2} <$   
20 4 vol.% in the early generation and up to 11 vol.% in later fluids). The important conclusions  
21 from that study are that the aqueous and carbonic fluids represent simultaneous trapping of  
22 heterogeneous fluids, and that variations in fluid density reflect changing conditions of  
23 hydrostatic vs. lithostatic pressure in the ductile shear zone. Nwe and Grundmann (1990)  
24 attributed the higher  $\text{CO}_2$  contents in the later fluid inclusions to consumption of  $\text{H}_2\text{O}$  by  
25 hydration reactions during advancement of the metasomatic front. Given the close association  
26 of emerald and tourmaline porphyroblasts in the blackwall zones and the similarity of their  
27 inclusion assemblages and zoning patterns, we can assume that the tourmalines studied here  
28 experienced the same fluctuations in fluid pressure and composition during growth.

29 There must be at least two isotopically distinct sources of boron to explain the variations  
30 in tourmaline isotope composition across the blackwall zones and within the growing crystals.  
31 The B-isotope composition of garnet-mica schist hosted tourmaline in the country rocks (-13  
32 to -10 ‰) is a typical value for continental metasediments (Palmer and Swihart, 1996;  
33 Kasemann et al., 2000) and one component in the Habachtal fluid-rock system is suggested to  
34 be crustal metamorphic fluid with this range of composition. The other boron source needed

1 to explain the tourmaline data must be isotopically heavy, and a conservative estimate for this  
2 component is -3 ‰ based on the highest observed  $\delta^{11}\text{B}$  values of -5 ‰ and using fluid-  
3 tourmaline fractionation factors for 500°C. This composition is in the range for MORB and  
4 altered oceanic crust (Palmer and Swihart, 1996) and given the geologic setting, the likely  
5 source of isotopically heavy boron is the serpentinite and metabasic rocks in the Habach  
6 Group (compare Altherr et al., 2004 and Marschall et al., 2007). In support of this suggestion  
7 is the regional association of blackwall alteration and serpentinite bodies in the Tauern  
8 Window distributed along the Greiner shear zone (Fig. 1a), which are interpreted as remnants  
9 of oceanic lithosphere caught up during the Alpine orogeny (Melcher et al., 2002). Barnes et  
10 al. (2004) argued from H and O isotope evidence that dehydration of serpentinites was an  
11 important source of fluids for blackwall-type metasomatism in the western Greiner shear  
12 zone, and this is consistent with our B-isotope results from the Habachtal.

13 We therefore propose that the main control on B-isotope variations in the Habachtal  
14 tourmalines is related to changing proportions of fluids from these two contrasting sources.  
15 The progressive shift towards heavier  $\delta^{11}\text{B}$  values from the country rock through transitional  
16 samples and into the blackwall alteration zones (Fig. 9) reflects the increasing fluid/rock  
17 ratios and greater dominance of heavy boron from the serpentinite/metabasite component. The  
18 isotopic scatter within individual samples can be explained by changing proportions of the  
19 component fluids in the shear zone with additional variations resulting from fractionation  
20 effects related to mineralization (of biotite, particularly) and increasing temperature. The trend  
21 toward isotopically lighter B in the rims of zoned tourmalines, which is observed in the  
22 blackwall and in the transitional samples, suggests a greater role of the regional metamorphic  
23 fluid at peak conditions.

24

## 25 **Conclusions**

26 The Habachtal emerald deposit is the type example of schist-hosted emerald deposits related  
27 to regional metamorphism. Deformation-enhanced metasomatic reactions between  
28 serpentinite and metapelitic country rocks in a ductile shear zone produced meter-thick  
29 “blackwall” alteration zones of biotite and chlorite schists which host the emerald  
30 mineralization. Tourmaline occurs in association with emerald in the blackwall zones and it is  
31 also a common accessory mineral in the country rock garnet-mica schists. Electron  
32 microprobe and SIMS analyses of tourmalines from an idealized profile across the blackwall  
33 sequence reveals systematic chemical and B-isotopic variations. Systematic chemical  
34 variations in tourmaline from unaltered country rock through transitional samples and into the



1 nearly monomineralic biotite and chlorite schists from the blackwall zones (decreasing Al and  
2 Fe/(Mg + Fe) ratio, increasing F and Cr) parallel changes in bulk composition of the rocks.  
3 Optical zoning is well developed in the blackwall tourmalines, and many grains also show  
4 strong compositional zoning, with increasing Mg, Ti, Ca and F concentration and decreasing  
5 Na and Al from core to rim, which mimics the differences found in the spatial sequence of  
6 blackwall zones. A special feature of some metasomatic tourmalines in the chlorite schist  
7 zone is development of hourglass sector zoning, with enrichments of Ti and Ca on opposite  
8 ends of the C axis. B-isotopic variations between the C<sup>+</sup> and C<sup>-</sup> sectors of these tourmalines  
9 are weak but significant, with a contrast on the order of 1.5‰.

10 The total range in B-isotope composition of Habachtal tourmalines is from -13.8 ‰ to -  
11 5.1 ‰ in the δ<sup>11</sup>B notation. Many of the optically and chemically zoned tourmalines from the  
12 blackwall and transitional zones also show a consistent trend of isotopic zoning, with the rims  
13 being isotopically lighter than the cores. The largest within-grain variation found was 4 ‰ but  
14 typically, the core-rim differences are about 1.5 to 2‰. Isotopic zoning is important, because  
15 when the core compositions are compared we find a systematic shift in δ<sup>11</sup>B values of  
16 tourmalines from the country rock (-14 to -10‰) to the inner blackwall zones (-9 to -5‰).  
17 This difference cannot be explained by Rayleigh fractionation or temperature variations, and  
18 we conclude there must be at least two contrasting boron sources. The simplest model that fits  
19 observed tourmaline compositions and is consistent with the geologic setting invokes two  
20 separate fluids that were channeled and partially mixed in the shear zone which hosts the  
21 Habachtal deposit. One is a regional metamorphic fluid with isotopically light boron as in the  
22 metapelite country rocks, and the other fluid is derived from the serpentinite association,  
23 which has isotopically heavy boron as in MORB or altered oceanic crust.

24

## 25 **Acknowledgements**

26 Several colleagues at the GFZ Potsdam contributed their technical expertise to this project.  
27 Gerhard Berger prepared the excellent polished thin sections, Oona Appelt set up and helped  
28 run the electron microprobe analyses and Ilona Schäpan assisted in the SIMS laboratory. Our  
29 special thanks go to Dieter Rhede for performing the high-resolution element mapping with  
30 the JEOL Hyperprobe. We are grateful for helpful reviews by Horst Marschall and Bill  
31 Leeman, which led to significant improvements in the paper.

32

## 33 **References**

34 Altherr R, Topuz G, Marschall H, Zack T, Ludwig T (2004) Evolution of a tourmaline-  
35 bearing lawsonite eclogite from the Elekdag area (Central Pontides, N Turkey): evidence

- 1 for infiltration of slab-derived B-rich fluids during exhumation. *Contrib Min Petrol* 148:  
2 409-425
- 3 Barnes JD, Selverstone J, Sharp Z (2004) Interactions between serpentinite devolatilization,  
4 metasomatism and strike-slip strain localization during deep-crustal shearing in the  
5 Eastern Alps. *J Met Geol* 22: 283-300
- 6 Bebout GE, Barton MD (2002) Tectonic and metasomatic mixing in a highT subduction-zone  
7 mélange - insights into the geochemical evolution of the slab-mantle interface. *Chem Geol*  
8 187: 79-106
- 9 Bebout G, Nakamura E (2003) Record in metamorphic tourmalines of subduction-zone  
10 devolatilization and boron cycling. *Geology* 31: 407-410
- 11 Bucher K, de Capitani C, Grapes R (2005) The development of a margarite-corundum  
12 blackwall by metasomatic alteration of a slice of mica schist in ultramafic rocks,  
13 Kvesjoen, Norwegian Caledonides. *Can Mineral* 43: 129-156
- 14 Catanzaro EJ, Champion CE, Garner EL, Maienko G, Sappenfield KM, Shields WR (1970)  
15 Boric Acid: Isotopic and Assay Standard Reference Materials. National Bureau Standards  
16 (US) Spec Publ 260-17: 70 p
- 17 Christensen JN, Selverstone J, Rosenfeld J., dePaolo DJ (1994) Correlation by Rb-Sr  
18 geochronology of garnet growth histories from different structural levels within the  
19 Tauern Window, Eastern Alps. *Contrib Mineral Petrol* 118: 1-12
- 20 Cliff RA (1981) Pre-Alpine history of the Pennine zone in the Tauern Window, Austria: U-Pb  
21 and Rb-Sr geochronology. *Contrib Mineral Petrol* 77: 262-266
- 22 Curtis CD, Brown PE (1969) The metasomatic development of zoned ultrabasic bodies in  
23 Unst, Shetland. *Contrib Mineral Petrol* 24: 275-292
- 24 Dyar MD, Wiedenbeck M, Robertson D, Cross LR, Delaney JS, Ferguson K, Francis CA,  
25 Grew ES, Guidotti CV, Hervig RL, Hughes JM, Husler J, Leeman W, McGuire AV,  
26 Rhede D, Rothe H, Paul RL, Richards I, Yates M. (2001) Reference Minerals for  
27 Microanalysis of Light Elements. *Geostandard Newsl* 25: 441-463
- 28 Groat LA, and 14 others (2002) Mineralogical and geochemical study of the Regal Ridge  
29 emerald showing, southeastern Yukon. *Can Mineral* 40: 1313-1338
- 30 Grundmann G. (1983) Die Genese der regionalmetamorphen, metasomatisch-  
31 horizontgebundenen Beryll-Mineralisationen des Habachtals, Land Salzburg, Österreich.  
32 Dissertation TU Berlin D83: 207 p
- 33 Grundmann G. (1989) Metamorphic evolution of the Habach Formation - a review. *Österr*  
34 *Mineral Gesell Mitt* 82: 75-88
- 35 Grundmann G. (1991) Smaragd. Grünes Feuer unterm Eis. Extra Lapis, 1, Christian Weise  
36 Verlag, München, 96 p
- 37 Grundmann G, Morteani G (1982) Die Geologie des Smaragdorkommens im Habachtal  
38 (Land Salzburg, Österreich). *Archive für Lagerstättenforschung Geologische*  
39 *Bundesanstalt Wien* 2: 71-107
- 40 Grundmann G, Morteani G (1989) Emerald mineralization during regional metamorphism:  
41 The Habachtal (Austria) and Leydsdorp (Transvaal, South Africa) deposits. *Econ Geol* 84:  
42 1835-1849
- 43 Hawthorne FC, Henry DJ (1999) Classification of the minerals of the tourmaline group. *Eur J*  
44 *Mineral* 11: 201-215
- 45 Henry DJ, Dutrow BL (1996) Metamorphic tourmaline and its petrologic applications. *Miner*  
46 *Soc Am Rev Mineral* 33: 503-558
- 47 Henry DJ, Guidotti CV (1985) Tourmaline as a petrogenetic indicator mineral: an example  
48 from the staurolite-grade metapelites of NW Maine. *Am Mineral* 70: 1-15
- 49 Hoernes S, Friedrichsen H (1974) Oxygen isotope studies on metamorphic rocks of the  
50 western Hohe Tauern area (Austria). *Schweiz Min Petr Mitt* 54: 769-788

- 1 Kasemann S, Erzinger J, Franz G (2000) Boron recycling in the continental crust of the  
2 central Andes from the Palaeozoic to Mesozoic, NW Argentina. *Contrib Mineral Petrol*  
3 140: 328-343
- 4 King RL, Kohn MJ, Eiler JM (2003) Constraints on the petrologic structure of the subduction  
5 zone slab-mantle interface from Franciscan Complex exotic ultramafic blocks. *Geol Soc*  
6 *Am Bull* 115: 1097-1109
- 7 Marschall HR, Ludwig T, Altherr R, Kalt A, Tonarini S (2006) Syros metasomatic  
8 tourmaline: evidence for very high- $\delta^{11}\text{B}$  fluids in subduction zones. *J Petrol* 47: 1915-  
9 1942
- 10 Melcher F, Meisel T, Puhl J, Koller F (2002) Petrogenesis and geotectonic setting of  
11 ultramafic rocks in the Eastern Alps: constraints from geochemistry. *Lithos* 65: 69-112
- 12 Meyer C, Wunder B, Meixner A, Romer RL, Heinrich W (2008) Boron-isotope fractionation  
13 between tourmaline and fluid: an experimental re-investigation. *Contrib Mineral Petrol*  
14 156: 259-267
- 15 Morteani G (1974) Petrology of the Tauern Window, Austrian Alps. *Fortschritt Mineral* 52:  
16 195-220
- 17 Morteani G, Grundmann G (1977) The emerald porphyroblasts in the penninic rocks of the  
18 Tauern Window, Austrian Alps. *N Jb Mineral Mh* 11: 509-516.
- 19 Nwe YY, Grundmann G (1990) Evolution of metamorphic fluids in shear zones: the record  
20 from the emeralds of Habachtal, Tauern Window, Austria. *Lithos* 25: 281-304
- 21 Okrusch M, Richter P, Guerkan A (1981) Geochemistry of blackwall sequences in the  
22 Habachtal emerald deposits, Hohe Tauern, Part 1: Presentation of geochemical data.  
23 *Tschermak Min Petr Mitt* 29: 9-31
- 24 Palmer MR, London D, Morgan GB VI, Babb HA (1992) Experimental determination of  
25 fractionation of  $^{11}\text{B}/^{10}\text{B}$  between tourmaline and aqueous vapor. A temperature and  
26 pressure-dependent isotopic system. *Chem Geol* 101: 123-129
- 27 Palmer MR, Swihart GH (1996) Boron isotope geochemistry: an overview. *Miner Soc Am*  
28 *Rev Mineral* 33: 709-744
- 29 Phillips AH, Hess HH (1936) Metamorphic differentiation at contacts between serpentinite  
30 and siliceous country rocks. *Am Mineral* 21: 333-362
- 31 Pouchou JL, Pichoir F (1984) An new model of quantitative X-ray microanalysis - part 1:  
32 Application to the analysis of homogeneous samples. *Rech Aerosp* 3: 13-38
- 33 Schmidt C, Thomas R, Heinrich W (2005) Boron speciation in aqueous fluids at 22 to 600°C  
34 and 0.1 MPa to 2 Gpa. *Geochim Cosmochim Acta* 69: 275-281
- 35 Seifert AV, Zacez V, Vrana S, Pecina V, Zacharias J, Zwaan JC (2004) Emerald  
36 mineralization in the Kafubu Area, Zambia. *Czech Geol Surv Bull Geosci* 79: 1-40
- 37 Tonarini S, Pennisi M, Adorni-Braccesi A, Dini A, Ferrara G, Gonfiantini R, Wiedenbeck M,  
38 Gröning M (2003) Intercomparison of Boron isotope and concentration measurements.  
39 Part I: Selection, preparation and homogeneity tests of the intercomparison materials.  
40 *Geostandard Newsl* 27: 21-39
- 41 Trumbull RB, Krienitz M-S, Gottesmann B, Wiedenbeck M (2008) Chemical and boron-  
42 isotope variations in tourmalines from an S-type granite and its source rocks: the Erongo  
43 granite and tourmalinites in the Damara Belt, Namibia. *Contrib Mineral Petrol* 155: 1-18
- 44 Williams LB, Hervig RL, Holloway JR, Hutcheon I (2001) Boron isotope geochemistry  
45 during diagenesis. Part 1. Experimental determination of fractionation during illitization  
46 of smectite. *Geochim Cosmochim Acta* 65: 1769-1782
- 47 Wunder B, Meixner A, Romer RL, Wirth R, Heinrich W (2005) The geochemical cycle of  
48 boron: Constraints from boron isotope partitioning experiments between mica and fluid.  
49 *Lithos* 84: 206-216

- 1 van Hinsberg VJ, Schumacher JC, Kearns S, Mason PRD, Franz G (2006) Hourglass sector  
2 zoning in tourmaline and resultant major and trace element fractionation. *Am Mineral* 91:  
3 717-728
- 4 van Hinsberg VJ, Marschall HR (2007) Boron isotope and light element sector zoning in  
5 tourmaline: implications for the formation of B-isotope signatures. *Chem Geol* 238: 141-  
6 148
- 7 van Hinsberg, VJ, Schumacher JC (2007) Intersector chemical partitioning in tourmaline: a  
8 potentially powerful single crystal thermometer. *Contrib Mineral Petrol* 153: 289-301  
9

## 10 **Figure Captions**

11 Figure 1. (a) Location map of the Tauern Window in the eastern Alps, Austria, showing the  
12 important tectonic units: central gneisses, Lower Schist Cover and Upper Schist Cover.  
13 The Habach Group which hosts the deposit is part of the Lower Schist Cover. Also shown  
14 with the "s" pattern is the ductile Greiner shear zone, which cuts through the central  
15 gneisses and hosts several serpentinite bodies along it. The Habachtal deposit (profile  
16 symbol) occurs along strike of the Greiner shear zone at the tectonic contact between the  
17 central gneisses (Habachzunge) and the Lower Schist Cover. (b) Lithologic cross section  
18 of the Habachtal deposit after Grundmann and Morteani (1989). On the W-side of the  
19 profile is the tectonic contact between the granitic orthogneisses of the Habachzunge and  
20 banded gneisses and amphibolites of the Habach Group. Metasomatic blackwall zones are  
21 developed in highly-sheared melange zones surrounding tectonic lenses of the  
22 "serpentinite-talc series". The emerald mineralization and the occurrence of tourmaline is  
23 confined to the eastern side of the profile in tectonic melange at contacts with the  
24 metapelitic unit in the Habach Group (garnet-mica schist series).

25 Figure 2. Schematic sketch of the blackwall zones between serpentinite and garnet-mica  
26 schist, with the location of samples used from this study. The chemical profiles shown for  
27 Cr and  $X_{Fe}$  represent whole-rock compositional trends given by Grundmann (1983).

28 Figure 3. Metamorphic crystallization/deformation diagram for plagioclase, tourmaline and  
29 beryl porphyroblasts in the blackwall-zone rocks in the Habachtal deposit, compiled from  
30 published structural, petrographic and microtextural analyses (Morteani and Grundmann,  
31 1977; Grundmann, 1983; 1991; Grundmann and Morteani, 1982; 1989). All stages  
32 depicted pertain to the Alpine metamorphic event.

33 Figure 4. Representative photomicrographs of tourmaline occurrences in rocks from the  
34 Habachtal deposit. **(a)** garnet-mica schist (sample 103b) with tourmaline crystals in quartz  
35 showing a pre-Alpine broken core (brown) which is healed and overgrown by blue  
36 Alpine-stage tourmaline; **(b)** another example of strong brittle deformation in pre-Alpine  
37 tourmaline with crack-fillings related to the Alpine event (sample 103b); **(c)** Garnet-mica

1 schist (sample 103b) showing a typical fine grained, polygonal tourmaline aggregate of  
2 pre-Alpine age (brown), which clearly predates development of the Alpine crenulation  
3 cleavage in the rock; **(d)** tourmaline grain aggregate in biotite-muscovite schist (sample  
4 AST-2) showing recrystallization fabrics. Very fine grained polygonal tourmaline  
5 aggregates (dark brown) overgrow columnar tourmaline porphyroblasts (light brown)  
6 indicating strain-induced grain boundary migration and reduction during the Alpine  
7 metamorphism; **(e)** zoned, euhedral tourmaline blast in biotite-chlorite schist from the  
8 blackwall zone with sigmoidal inclusion trails indicating tourmaline growth during Alpine  
9 deformation. **(f)** a typical zoned euhedral tourmaline from blackwall biotite-chlorite schist  
10 with an inclusion-rich core and inclusion-poor rim; **(g)** hourglass sector zoning in a  
11 tourmaline blast from chlorite schist (sample 103a, grain C-T2). The lighter-colored  
12 antigorite pole ( $C^+$ ) is poor in Ti, Ca and Mg compared with the analogous ( $C^-$ ) pole; **(h)**  
13 element map of Ti distribution for the sector-zoned crystal shown in (g) acquired by  
14 electron microprobe. The warmer colors represent higher Ti concentrations.

15 Figure 5. Classification diagrams for the tourmalines from the Habachtal deposit, based on the  
16 principal constituent at the X-site (Hawthorne and Henry, 1999) in (a); and on the Al-Fe-  
17 Mg ternary diagram from Henry and Guidotti (1985) in (b). The labelled fields in plot (b)  
18 are: (1) Li-rich granitoid pegmatites and aplites, (2) Li-poor granitoids, pegmatites and  
19 aplites, (3)  $Fe^{3+}$ -rich quartz-tourmaline rocks (altered granitoids), (4) metapelites and  
20 metapsammites with Al-saturating phase, (5) metapelites and metapsammites lacking Al-  
21 saturating phase, (6)  $Fe^{3+}$ -rich quartz-tourmaline rocks, calc-silicate rocks and metapelites,  
22 (7) low-Ca metaultramafic rocks and Cr-V-rich metasediments, (8) metacarbonates and  
23 metapyroxenites.

24 Figure 6. Chemical compositions of tourmalines from the Habachtal deposit expressed in  
25 terms of the atomic ratios  $Fe/(Fe+Mg)$  versus (a)  $Na/(Na+Ca)$  and (b) F (wt.%); and in (c)  
26 contents of CaO (wt.%) vs.  $TiO_2$  (wt.%). Whole rock ranges shown in (a) are from data in  
27 Grundmann (1983).

28 Figure 7. Compositional variation diagrams of (a) total Al (atoms per formula unit) and (b) X-  
29 site vacancies versus Fe (atoms p.f.u.); exchange vectors are indicated by arrows ( $\square$  -  
30 vacancy).

31 Figure 8. An example of tourmaline compositional zoning from blackwall-zone samples. The  
32 tielines connect core and rim compositions of individual tourmaline grains analyzed in  
33 sample 103a (chlorite schist).

1 Figure 9. Frequency histograms of boron isotope compositions of Habachtal tourmalines from  
2 the country rock, transition zone and blackwall zone samples. The core and rim  
3 compositions of zoned grains are shown separately. The error bar in the upper panel  
4 illustrates the analytical repeatability of SIMS analyses at the  $2\sigma$  level. The shaded zone  
5 emphasizes the observed trend to higher  $\delta^{11}\text{B}$  values with increasing intensity of blackwall  
6 alteration. This trend is found in tourmaline cores, meaning a shift in fluid composition  
7 during tourmaline growth.

Table 1. Results of SIMS B-isotope analyses on reference tourmalines.

Analysis Date	$^{11}\text{B}/^{10}\text{B}$	1sd (‰) <sup>a</sup>	IMF <sup>b</sup>	$\delta^{11}\text{B}$ (‰) <sup>c</sup>	Analysis Date	$^{11}\text{B}/^{10}\text{B}$	1sd (‰) <sup>a</sup>	IMF <sup>b</sup>	$\delta^{11}\text{B}$ (‰) <sup>c</sup>
Dravite ( $^{11}\text{B}/^{10}\text{B} = 4.017$ and $\delta^{11}\text{B} = -6.6$ )					Dravite ( $^{11}\text{B}/^{10}\text{B} = 4.017$ and $\delta^{11}\text{B} = -6.6$ )				
12/13/2006	3.830	0.35	0.9535	-5.9	<b>3/26/2007</b>	<b>3.828</b>	<b>0.28</b>	<b>0.9530</b>	<b>-4.4</b>
12/13/2006	3.828	0.32	0.9530	-6.4	3/26/2007	3.817	0.31	0.9502	-7.3
12/13/2006	3.827	0.30	0.9527	-6.7	3/27/2007	3.813	0.37	0.9492	-8.3
12/14/2006	3.826	0.30	0.9525	-6.9	3/27/2007	3.818	0.36	0.9505	-7.0
12/14/2006	3.825	0.30	0.9522	-7.2	3/27/2007	3.815	0.32	0.9497	-7.8
Mean	3.827			-6.6	Mean	3.816			-7.6
Repeatability in permil <sup>d</sup>	0.50				Repeatability in permil <sup>d</sup>	0.58			
Schorl ( $^{11}\text{B}/^{10}\text{B} = 3.993$ and $\delta^{11}\text{B} = -12.5$ )					Schorl ( $^{11}\text{B}/^{10}\text{B} = 3.993$ and $\delta^{11}\text{B} = -12.5$ )				
12/13/2006	3.805	0.31	0.9529	-11.9	<b>3/26/2007</b>	<b>3.807</b>	<b>0.28</b>	<b>0.9534</b>	<b>-9.9</b>
12/13/2006	3.803	0.25	0.9524	-12.4	3/27/2007	3.793	0.45	0.9499	-13.5
12/14/2006	3.801	0.26	0.9519	-12.9	3/27/2007	3.797	0.45	0.9509	-12.5
12/14/2006	3.800	0.29	0.9516	-13.2	3/27/2007	3.797	0.45	0.9509	-12.5
Mean	3.802			-12.6	Mean	3.796			-12.8
Repeatability in permil <sup>d</sup>	0.58				Repeatability in permil <sup>d</sup>	0.61			
Elbaite ( $^{11}\text{B}/^{10}\text{B} = 4.001$ and $\delta^{11}\text{B} = -10.4$ )					<b>Values in bold type are outliers and not used in repeatability or IMF calculations</b>				
12/13/2006	3.804	0.36	0.9507	-9.5					
12/13/2006	3.805	0.28	0.9509	-9.2					
12/13/2006	3.804	0.35	0.9507	-9.5					
12/14/2006	3.801	0.34	0.9499	-10.3					
12/14/2006	3.796	0.34	0.9487	-11.6					
Mean	3.802			-10.0					
Repeatability in permil <sup>d</sup>	1.06								
B4 tourmaline ( $^{11}\text{B}/^{10}\text{B} = 4.0078$ and $\delta^{11}\text{B} = -8.9$ )									
12/13/2006	3.820	0.30	0.9531	-8.4					
12/13/2006	3.820	0.29	0.9531	-8.4					
12/13/2006	3.818	0.28	0.9526	-9.0					
12/14/2006	3.819	0.32	0.9529	-8.7					
12/14/2006	3.815	0.31	0.9519	-9.7					
Mean	3.818			-8.9					
Repeatability in permil <sup>d</sup>	0.57								

a) Individual uncertainty for 100 cycles (standard deviation / mean)\*1000

b) Instrumental mass fractionation ( $^{11}\text{B}/^{10}\text{B}$  measured /  $^{11}\text{B}/^{10}\text{B}$  RM)

c) Calculated from ratios corrected with average IMF values of 0.9520 (Dec06) and 0.9506 (Mar07) and  $^{11}\text{B}/^{10}\text{B} = 4.04362$  for NBS SRM 951

d) Repeatability in permil from multiple analyses of each reference material (standard deviation / mean)\*1000

Table 2. Chemical analyses and B-isotope ratios of tourmalines from the Habachtal emerald deposit

Sample Position	M-26 (phengite schist, transition zone)									AST-2 (biotite-muscovite schist, transition zone)									102 (blackwall bt.-chl. schist)			
	core	rim	rim	core	core	rim	core	rim	core	rim	core	core	core	rim	interior	interior	interior	core	interior	rim	core	
SiO <sub>2</sub> (wt.%)	37.6	37.2	37.3	37.3	37.7	37.1	37.8	37.7	37.6	36.9	37.7	37.7	37.6	37.1	37.2	37.6	37.1	36.3	37.1	37.1	36.9	
TiO <sub>2</sub>	0.17	0.22	0.21	0.22	0.13	0.24	0.26	0.17	0.21	0.50	0.15	0.18	0.21	0.51	0.47	0.09	0.49	0.90	0.22	0.49	0.52	
Al <sub>2</sub> O <sub>3</sub>	31.7	31.7	31.1	31.2	32.0	31.7	31.0	31.4	31.6	30.3	31.7	31.4	30.9	30.8	30.0	31.3	29.8	29.6	31.7	30.0	30.4	
MgO	9.82	9.91	9.73	9.88	9.65	9.54	10.24	9.69	9.58	9.13	8.70	9.00	9.22	9.27	9.21	8.89	9.30	8.04	8.67	9.24	7.96	
MnO	0.03	0.02	0.02	0.04	0.04	0.03	0.04	0.01	0.04	0.00	0.01	0.02	0.05	0.03	0.00	0.01	0.03	0.00	0.03	0.01	0.02	
FeO	3.35	3.25	3.43	3.59	3.09	3.55	3.17	3.52	3.55	5.10	4.37	4.64	5.16	5.05	5.11	4.69	5.47	7.28	4.97	5.18	7.06	
Cr <sub>2</sub> O <sub>3</sub>	0.01	0.00	0.00	0.01	0.01	0.00	0.00	0.00	0.03	0.03	0.01	0.01	0.00	0.00	0.00	0.01	0.01	0.08	0.05	0.09	0.06	
CaO	0.71	0.90	0.86	0.95	0.38	0.80	0.62	0.78	0.69	0.99	0.40	0.42	0.28	1.01	1.00	0.34	0.75	0.81	0.37	0.83	0.62	
Na <sub>2</sub> O	2.44	2.32	2.34	2.36	2.60	2.37	2.53	2.44	2.45	2.35	2.25	2.49	2.74	2.25	2.31	2.51	2.51	2.43	2.43	2.40	2.55	
K <sub>2</sub> O	0.02	0.01	0.02	0.02	0.01	0.02	0.02	0.02	0.00	0.00	0.01	0.01	0.01	0.01	0.04	0.01	0.01	0.02	0.02	0.02	0.01	
F	0.00	0.00	0.00	0.00	0.00	0.00	0.20	0.00	0.00	0.00	0.00	0.00	0.03	0.01	0.00	0.00	0.17	0.37	0.11	0.12	0.20	
Cl	0.00	0.00	0.00	0.01	0.00	0.00	0.01	0.00	0.00	0.00	0.02	0.01	0.01	0.01	0.00	0.01	0.00	0.00	0.01	0.01	0.00	
Sum	85.8	85.6	85.0	85.6	85.6	85.3	85.9	85.7	85.7	85.3	85.3	85.9	86.2	86.0	85.3	85.5	85.7	85.9	85.6	85.4	86.3	
Si (Atoms p.f.u.)	6.087	6.044	6.113	6.086	6.106	6.056	6.132	6.126	6.117	6.093	6.161	6.133	6.114	6.059	6.134	6.151	6.110	6.055	6.059	6.112	6.089	
Al(T)	0.000	0.000	0.000	0.000	0.000	0.000	0.000	0.000	0.000	0.000	0.000	0.000	0.000	0.000	0.000	0.000	0.000	0.000	0.000	0.000	0.000	
Al(Z)	6.000	6.000	6.000	5.992	6.000	6.000	5.925	6.000	6.000	5.895	6.000	6.000	5.918	5.929	5.838	6.000	5.791	5.819	6.000	5.837	5.907	
Al(Y)	0.063	0.083	0.010	0.000	0.122	0.106	0.000	0.025	0.047	0.000	0.104	0.028	0.000	0.000	0.000	0.030	0.000	0.000	0.114	0.000	0.000	
Ti	0.021	0.027	0.026	0.027	0.016	0.029	0.032	0.020	0.026	0.062	0.019	0.022	0.026	0.063	0.059	0.011	0.060	0.113	0.027	0.060	0.064	
Mg	2.372	2.401	2.378	2.401	2.330	2.321	2.476	2.348	2.321	2.244	2.117	2.183	2.234	2.256	2.264	2.165	2.281	1.995	2.113	2.270	1.958	
Mn	0.003	0.003	0.003	0.005	0.006	0.004	0.005	0.002	0.005	0.000	0.001	0.002	0.006	0.004	0.000	0.002	0.004	0.000	0.004	0.001	0.003	
Fe	0.454	0.442	0.470	0.489	0.419	0.485	0.430	0.479	0.483	0.704	0.597	0.631	0.702	0.690	0.705	0.642	0.753	1.014	0.680	0.715	0.975	
Cr	0.001	0.000	0.000	0.001	0.001	0.000	0.000	0.000	0.002	0.002	0.001	0.001	0.000	0.000	0.000	0.001	0.001	0.005	0.003	0.006	0.004	
Ca	0.123	0.156	0.152	0.166	0.066	0.139	0.108	0.135	0.120	0.174	0.070	0.074	0.049	0.177	0.176	0.060	0.131	0.145	0.064	0.146	0.109	
Na	0.767	0.730	0.743	0.746	0.817	0.750	0.796	0.770	0.773	0.751	0.711	0.787	0.865	0.712	0.740	0.796	0.800	0.785	0.771	0.769	0.816	
K	0.004	0.002	0.004	0.004	0.002	0.004	0.003	0.005	0.000	0.000	0.002	0.002	0.003	0.001	0.008	0.001	0.003	0.005	0.004	0.005	0.002	
vacancies	0.105	0.112	0.101	0.085	0.115	0.106	0.092	0.090	0.107	0.075	0.218	0.138	0.084	0.109	0.076	0.143	0.066	0.065	0.161	0.081	0.073	
<sup>11</sup> B/ <sup>10</sup> B	4.013	4.003	3.991	3.994	4.001	4.000	4.000	3.994	3.995	3.995	4.002	4.006	4.019	3.992	4.013	4.004	4.016	4.022	4.011	4.018	4.022	
1σ uncertainty(‰)	0.36	0.36	0.35	0.31	0.36	0.32	0.38	0.33	0.35	0.33	0.31	0.34	0.32	0.35	0.34	0.32	0.35	0.33	0.34	0.29	0.35	
δ <sup>11</sup> B (‰)	-7.7	-10.0	-13.1	-12.3	-10.5	-10.8	-10.8	-12.3	-12.1	-12.1	-10.3	-9.2	-6.1	-12.9	-7.7	-9.7	-6.9	-5.3	-8.2	-6.4	-5.3	

Chemical analyses by electron microprobe, total Fe reported as FeO, structural formula based on 15 cations in T, Z and Y sites (Henry and Dutrow, 1996)

B-isotope ratios by SIMS on points adjacent to microprobe sites, corrected for instrumental mass fractionation (Table 1) and with 1 sigma individual uncertainty given in permil.



Table 2. (continued)

Sample Position	103c (blackwall bt. schist)				103a (blackwall chlorite schist)								103b (country rock ga.-mu. schist)					
	rim	interior	rim	core	rim	core	rim	core	rim	core	rim	rim	rim	core	interior	interior	core	core
SiO <sub>2</sub> (wt.%)	37.0	37.0	37.3	37.2	37.3	37.3	37.4	37.3	37.5	37.7	37.4	37.1	37.4	37.3	37.0	36.7	37.1	37.2
TiO <sub>2</sub>	0.50	0.60	0.50	0.35	0.43	0.32	0.52	0.13	0.47	0.20	0.22	0.60	0.35	0.10	1.07	0.90	0.71	0.66
Al <sub>2</sub> O <sub>3</sub>	30.1	30.5	30.8	30.5	30.2	30.2	30.8	31.5	30.7	31.4	31.7	30.5	30.6	31.3	31.8	32.3	33.2	32.7
MgO	9.42	9.37	9.71	9.17	9.59	9.35	9.67	8.68	9.88	8.97	8.91	9.58	9.60	8.54	6.31	6.44	6.18	5.60
MnO	0.00	0.02	0.02	0.06	0.00	0.01	0.00	0.01	0.00	0.00	0.03	0.01	0.01	0.00	0.04	0.06	0.06	0.09
FeO	4.97	4.71	3.97	5.55	3.91	4.05	3.85	4.34	3.86	4.22	4.33	3.95	3.91	5.36	8.33	7.94	7.54	8.11
Cr <sub>2</sub> O <sub>3</sub>	0.06	0.04	0.03	0.04	0.06	0.03	0.03	0.01	0.07	0.02	0.05	0.08	0.06	0.03	0.10	0.00	0.03	0.01
CaO	0.87	0.66	0.98	0.54	0.90	0.75	1.09	0.26	0.94	0.35	0.28	1.03	0.78	0.12	0.79	1.06	0.99	0.77
Na <sub>2</sub> O	2.45	2.53	2.30	2.55	2.51	2.58	2.24	2.48	2.41	2.45	2.49	2.30	2.58	2.71	2.11	1.99	1.87	1.86
K <sub>2</sub> O	0.02	0.02	0.03	0.03	0.02	0.00	0.02	0.03	0.02	0.00	0.01	0.02	0.02	0.02	0.02	0.03	0.02	0.02
F	0.03	0.25	0.21	0.04	0.32	0.21	0.31	0.00	0.41	0.09	0.14	0.27	0.25	0.00	0.00	0.00	0.00	0.00
Cl	0.00	0.01	0.00	0.01	0.01	0.00	0.01	0.00	0.00	0.00	0.01	0.01	0.01	0.00	0.01	0.00	0.01	0.01
Sum	85.4	85.7	85.9	86.1	85.3	84.7	85.9	84.8	86.2	85.3	85.5	85.4	85.6	85.5	87.6	87.5	87.7	87.0
Si (Atoms p.f.u.)	6.094	6.080	6.088	6.074	6.165	6.186	6.121	6.143	6.107	6.162	6.111	6.104	6.136	6.114	6.052	5.999	6.032	6.105
Al(T)	0.000	0.000	0.000	0.000	0.000	0.000	0.000	0.000	0.000	0.000	0.000	0.000	0.000	0.000	0.000	0.001	0.000	0.000
Al(Z)	5.844	5.899	5.939	5.881	5.877	5.898	5.930	6.000	5.903	6.000	6.000	5.921	5.928	6.000	6.000	6.000	6.000	6.000
Al(Y)	0.000	0.000	0.000	0.000	0.000	0.000	0.000	0.113	0.000	0.049	0.096	0.000	0.000	0.053	0.130	0.228	0.352	0.323
Ti	0.062	0.075	0.061	0.043	0.054	0.040	0.064	0.016	0.057	0.024	0.027	0.074	0.044	0.013	0.131	0.111	0.086	0.081
Mg	2.312	2.293	2.365	2.232	2.360	2.312	2.356	2.129	2.401	2.187	2.168	2.352	2.349	2.085	1.537	1.568	1.496	1.367
Mn	0.000	0.003	0.003	0.009	0.000	0.001	0.000	0.001	0.000	0.000	0.004	0.001	0.002	0.000	0.005	0.008	0.008	0.012
Fe	0.684	0.647	0.542	0.758	0.541	0.562	0.526	0.598	0.527	0.577	0.591	0.545	0.537	0.734	1.139	1.084	1.024	1.112
Cr	0.004	0.002	0.002	0.003	0.004	0.002	0.002	0.001	0.004	0.001	0.003	0.005	0.004	0.002	0.006	0.000	0.002	0.001
Ca	0.153	0.116	0.172	0.094	0.159	0.133	0.190	0.046	0.164	0.062	0.050	0.182	0.138	0.020	0.139	0.186	0.172	0.135
Na	0.781	0.805	0.729	0.807	0.803	0.829	0.710	0.790	0.762	0.778	0.788	0.735	0.822	0.862	0.667	0.630	0.589	0.590
K	0.004	0.004	0.005	0.007	0.004	0.001	0.003	0.006	0.004	0.001	0.002	0.003	0.005	0.003	0.003	0.007	0.005	0.004
vacancies	0.062	0.075	0.093	0.092	0.034	0.037	0.097	0.158	0.070	0.159	0.161	0.079	0.036	0.115	0.191	0.177	0.235	0.271
<sup>11</sup> B/ <sup>10</sup> B	4.016	4.018	4.005	4.015	4.008	4.020	4.007	4.011	4.007	4.022	4.020	4.002	4.005	4.023	4.004	3.989	3.996	3.996
1σ uncertainty (‰)	0.30	0.32	0.33	0.33	0.32	0.33	0.32	0.32	0.30	0.32	0.29	0.34	0.31	0.32	0.38	0.28	0.35	0.35
δ <sup>11</sup> B (‰)	-6.9	-6.4	-9.5	-7.1	-8.7	-5.8	-9.0	-8.2	-9.0	-5.3	-5.8	-10.3	-9.5	-5.1	-9.8	-13.5	-11.7	-11.7

Chemical analyses by electron microprobe, total Fe reported as FeO, structural formula based on 15 cations in T, Z and Y sites (Henry and Dutrow, 1996)

B-isotope ratios by SIMS on points adjacent to microprobe sites, corrected for instrumental mass fractionation (Table 1) and with individual uncertainty given in permil.

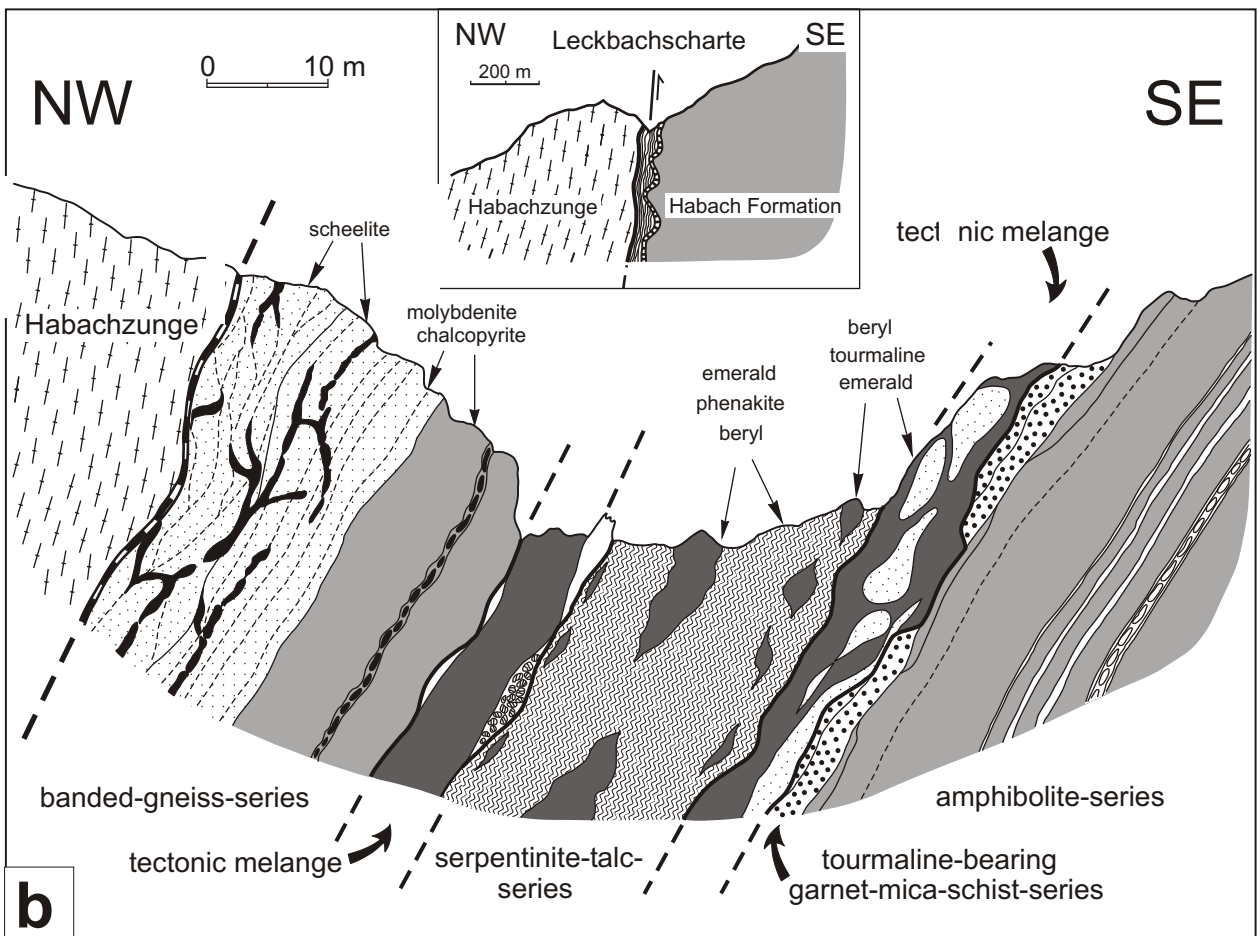
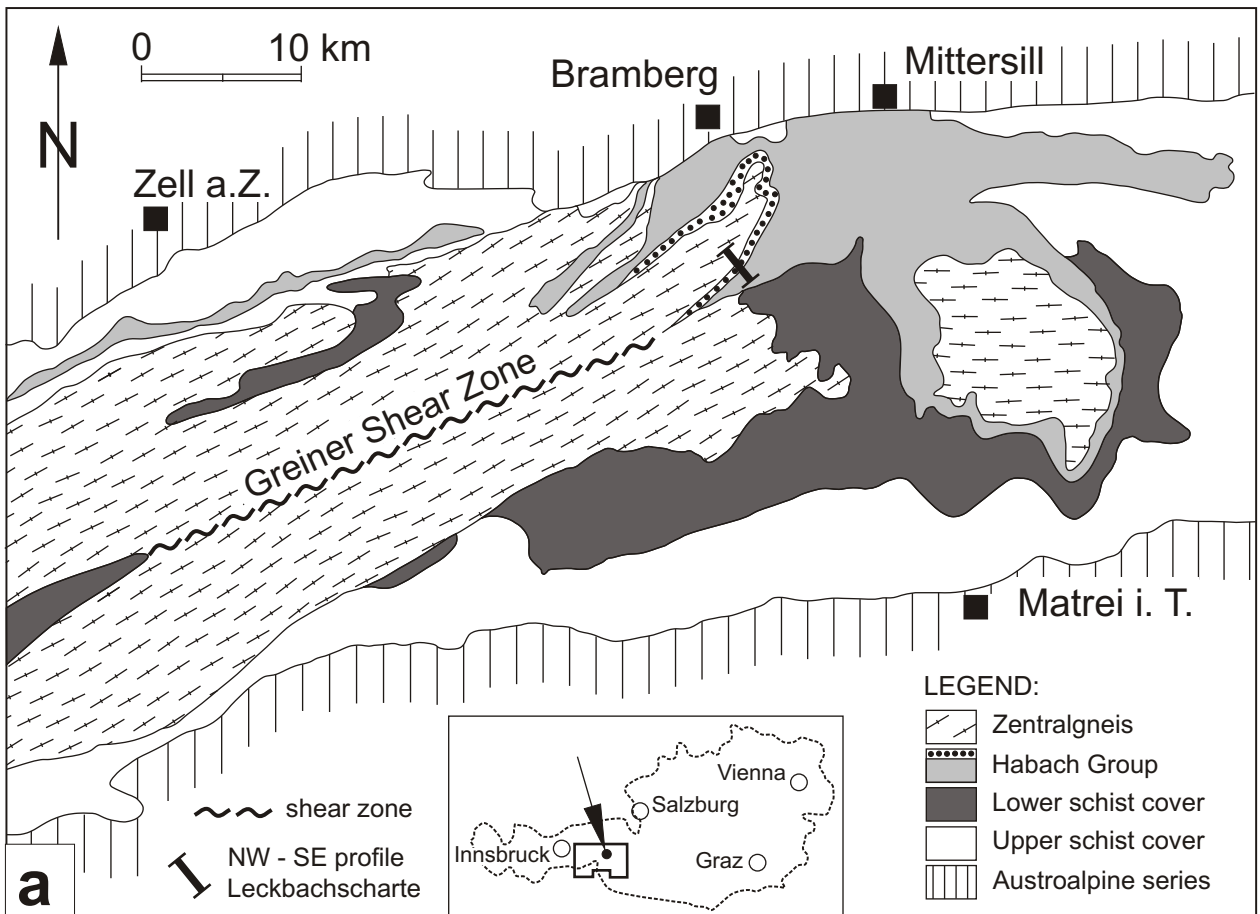
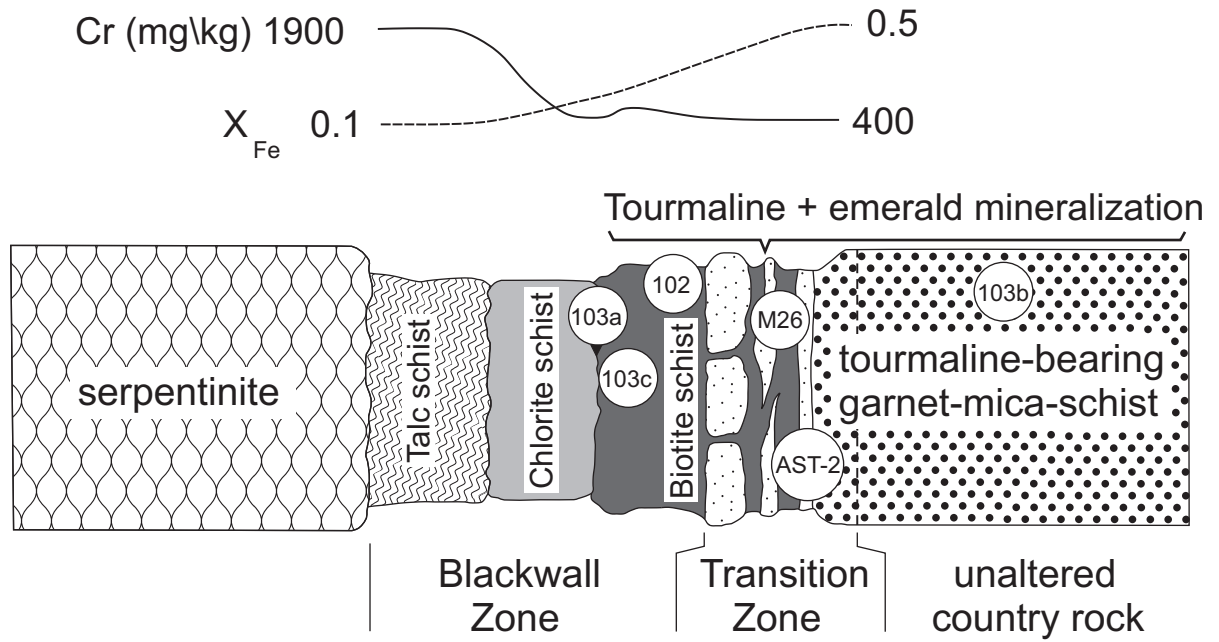


Fig. 1

Whole-rock variations



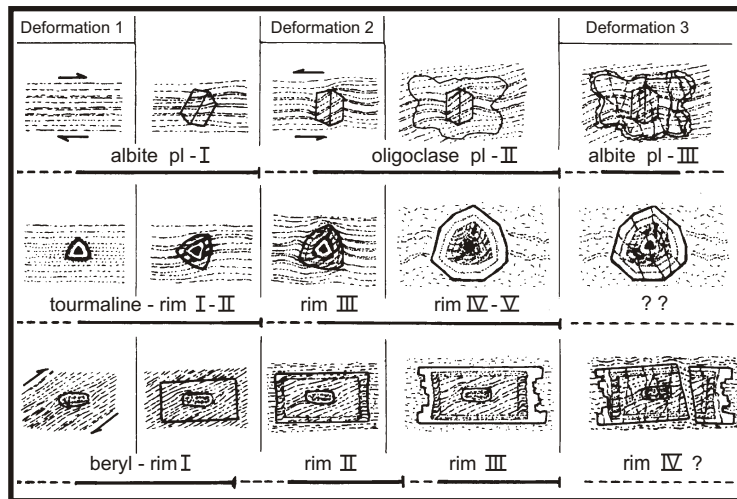


Fig. 3

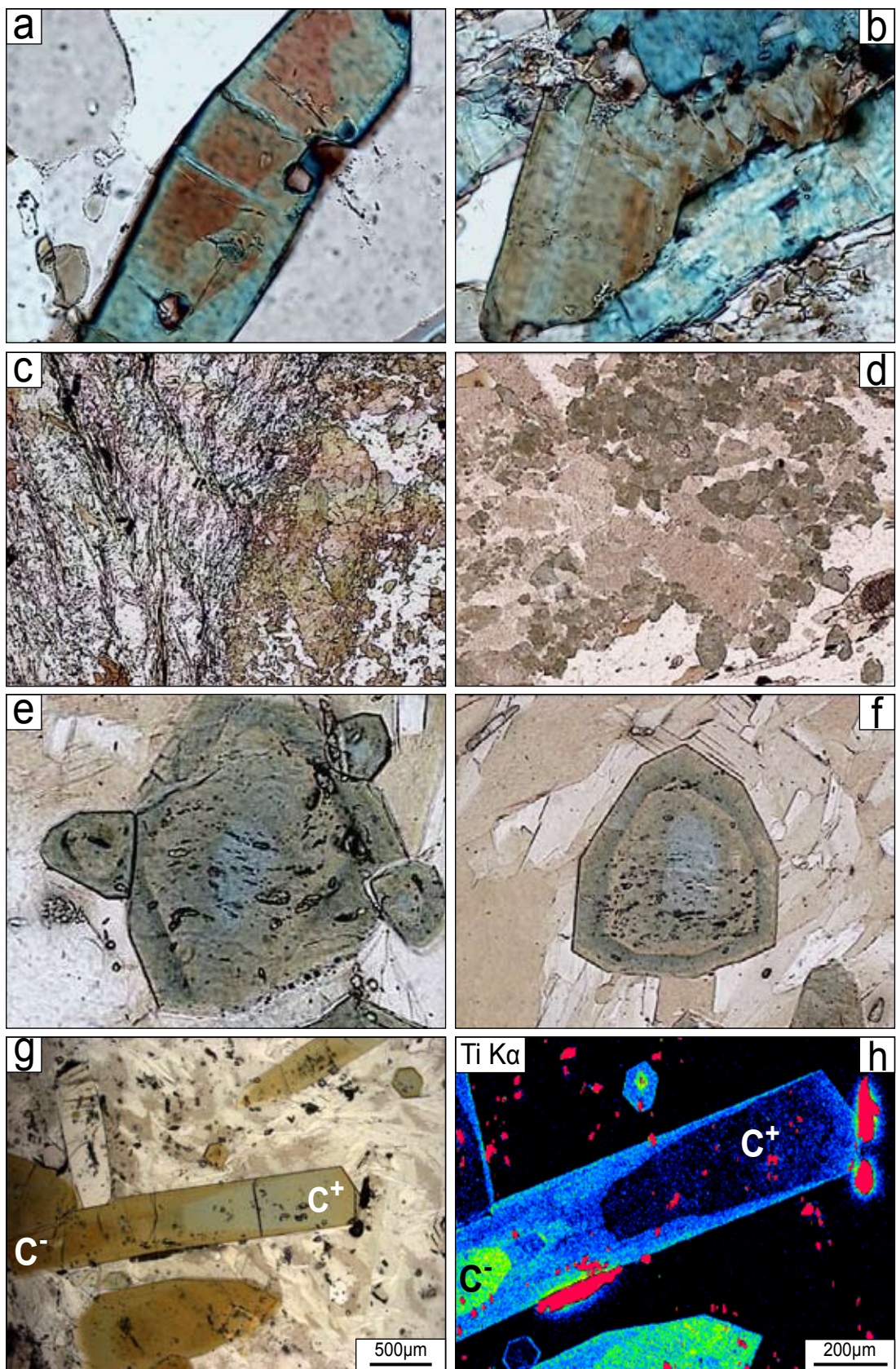


Figure 4

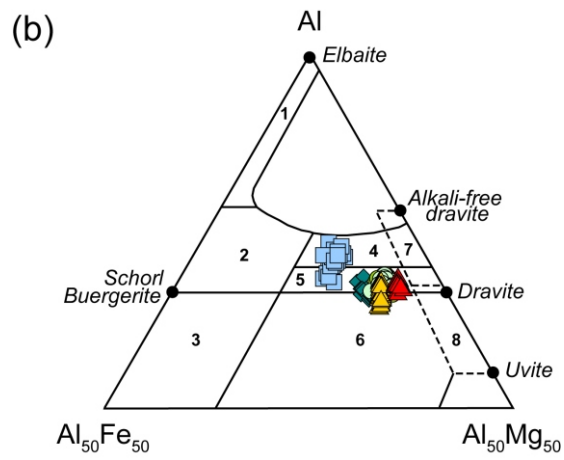
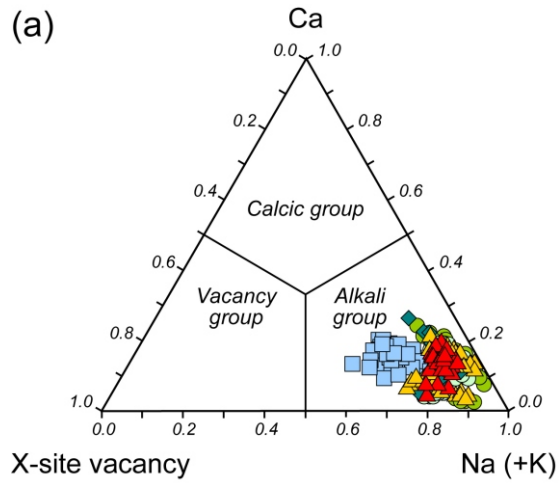


Fig. 5

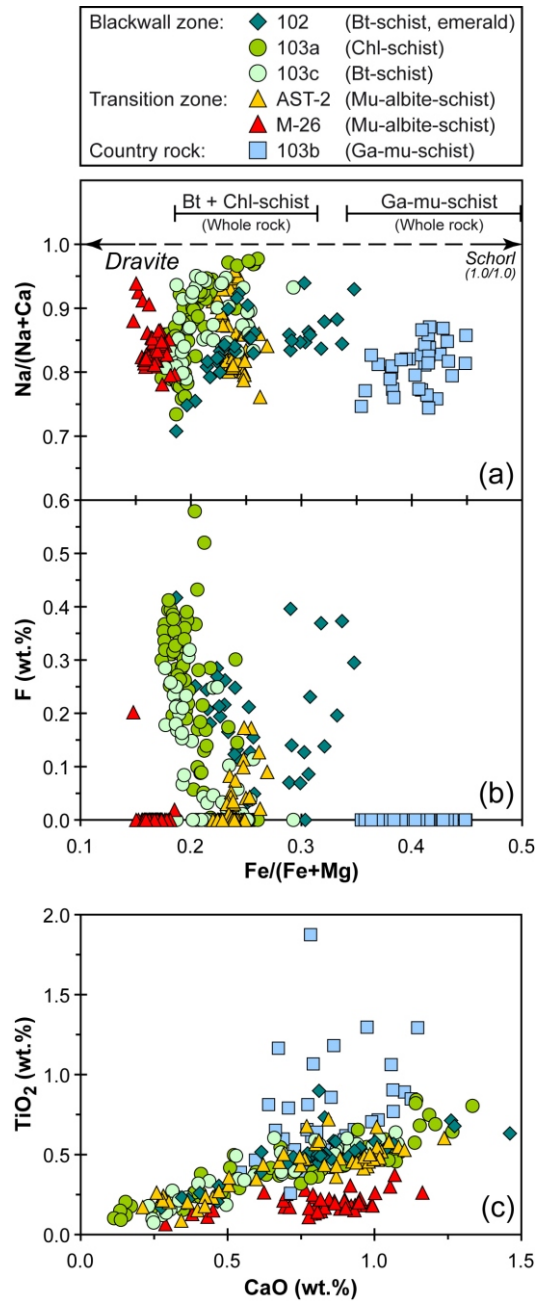


Fig. 6

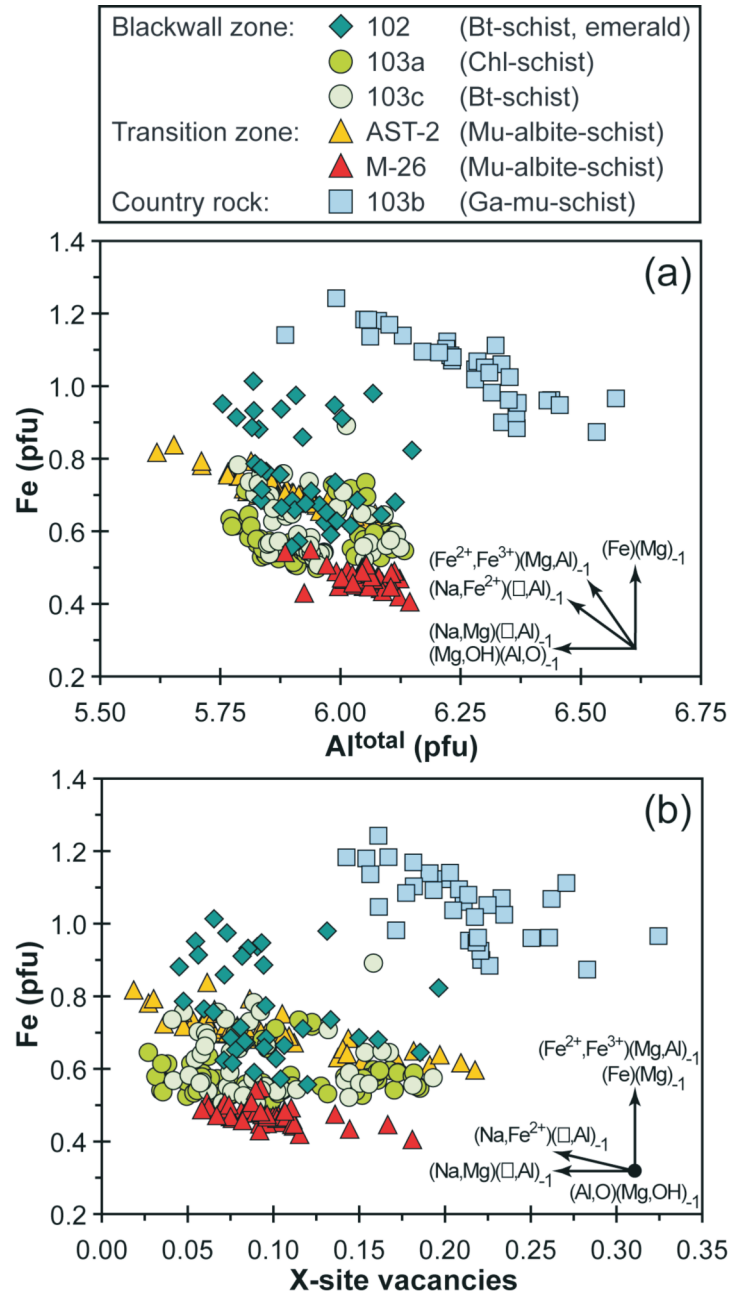


Fig. 7



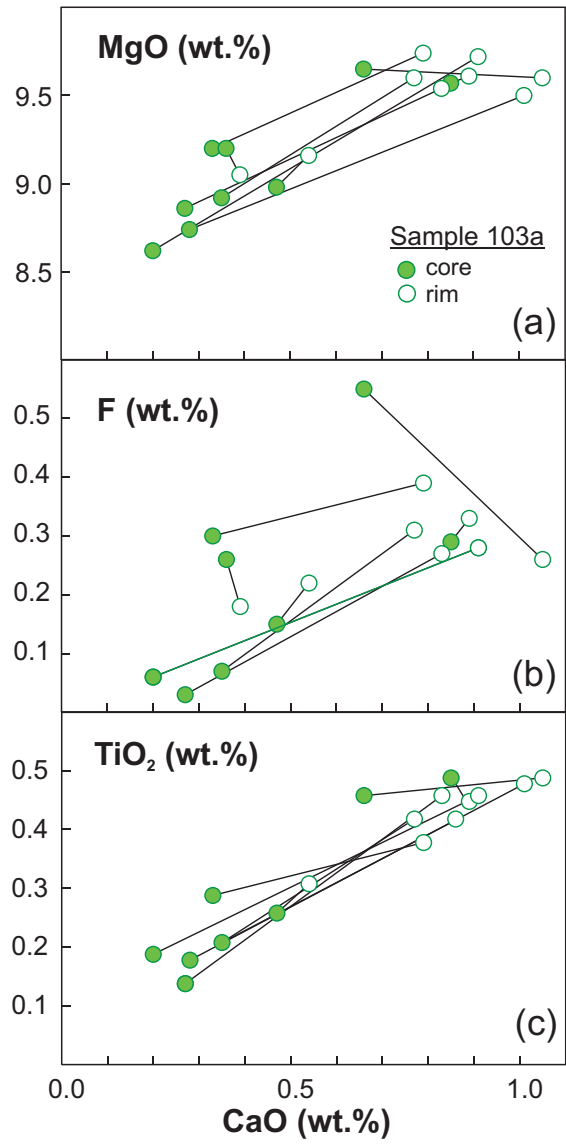


Fig. 8

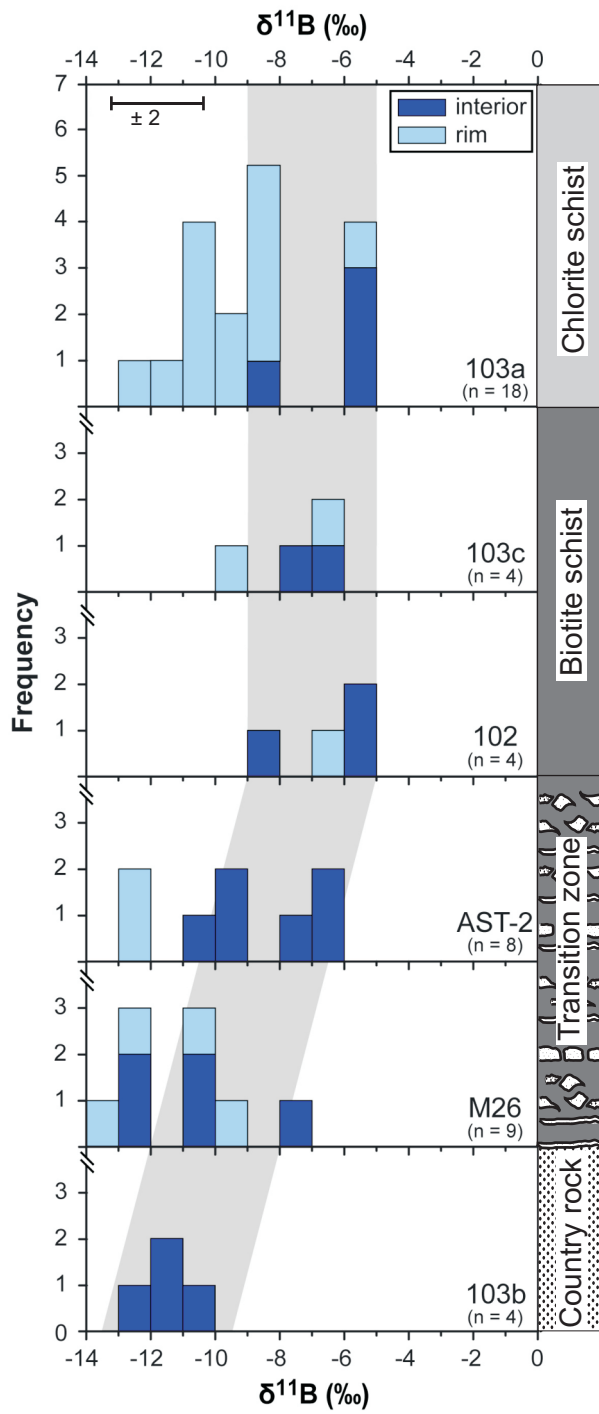


Fig. 9